

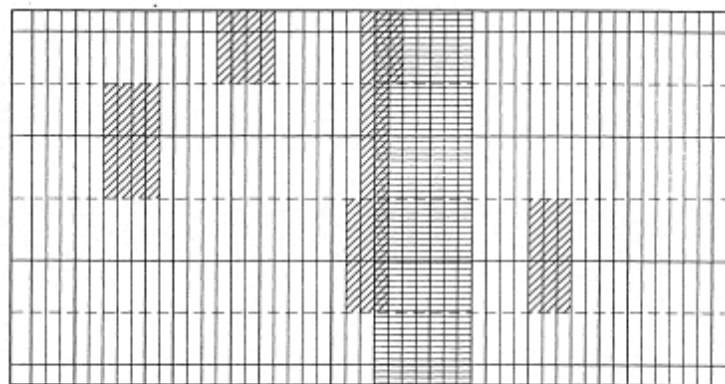
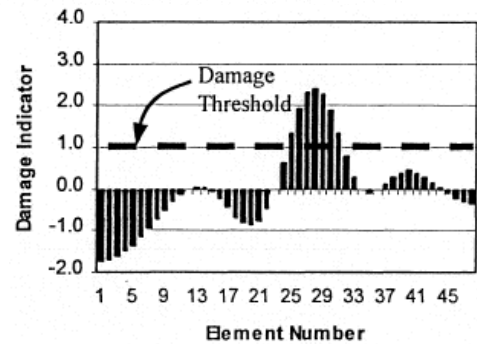
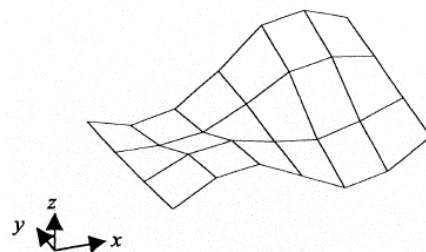
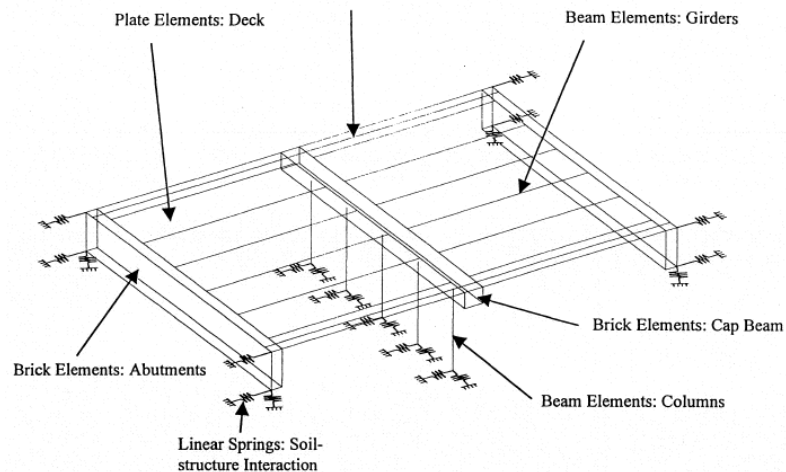


Division of Research  
& Innovation

# The Evaluation of Key System Performance Measures for the Kings Stormwater Crossing Bridge Using a Level IV Non-Destructive Damage Evaluation Method

System Identification and Damage Localization of the Kings Stormwater Channel Bridges

## Final Report



Possible Damage Locations Using Bending Mode     
 Possible Damage Locations Using Torsion Mode

# **The Evaluation of Key System Performance Measures for the Kings Stormwater Crossing Bridge Using a Level IV Non-Destructive Damage Evaluation Method**

System Identification and Damage Localization of the Kings Stormwater Channel Bridges

**Final Report**

**Report No. CA03-0130**

**December 2008**

*Prepared By:*

Texas Engineering Experiment Station  
Texas A&M University  
College Station, Texas 77843

*Prepared For:*

California Department of Transportation  
Engineering Services Center  
1801 30<sup>th</sup> Street  
Sacramento, CA 95816

California Department of Transportation  
Division of Research and Innovation, MS-83  
1227 O Street  
Sacramento, CA 95814

## **DISCLAIMER STATEMENT**

**This document is disseminated in the interest of information exchange. The contents of this report reflect the views of the authors who are responsible for the facts and accuracy of the data presented herein. The contents do not necessarily reflect the official views or policies of the State of California or the Federal Highway Administration. This publication does not constitute a standard, specification or regulation. This report does not constitute an endorsement by the Department of any product described herein.**

STATE OF CALIFORNIA DEPARTMENT OF TRANSPORTATION  
**TECHNICAL REPORT DOCUMENTATION PAGE**  
 TR0003 (REV. 10/98)

1. REPORT NUMBER CA03-0130		2. GOVERNMENT ASSOCIATION NUMBER		3. RECIPIENT'S CATALOG NUMBER	
4. TITLE AND SUBTITLE The Evaluation of Key Performance Measures for the Kings Stormwater Crossing Bridge Using a Level IV Non-Destructive Damage Evaluation Method: System Identification and Damage Localization of the Kings Stormwater Channel Bridges.				5. REPORT DATE December, 2008	
7. AUTHOR(S) Norris Stubbs, Sanghyun Choi, Robert Bolton, Charles Sikorsky				6. PERFORMING ORGANIZATION CODE	
9. PERFORMING ORGANIZATION NAME AND ADDRESS Texas Engineering Experiment Station Texas A&M University College Station, Texas 77843				8. PERFORMING ORGANIZATION REPORT NO. TEES Contract 32525-51640CE	
12. SPONSORING AGENCY AND ADDRESS California Department of Transportation Engineering Services Center 1801 30 <sup>th</sup> Street Sacramento, CA 95816  California Department of Transportation Division of Research and Innovation, MS-83 1227 O Street Sacramento, CA 95814				10. WORK UNIT NUMBER	
				11. CONTRACT OR GRANT NUMBER DRI Research Task No. 0130 Contract No. 59A0216	
15. SUPPLEMENTAL NOTES .				13. TYPE OF REPORT AND PERIOD COVERED Final Report	
				14. SPONSORING AGENCY CODE 913	
16. ABSTRACT The objective of this report is to describe the system identification and nondestructive damage evaluation of two recently constructed bridges in southern California. The first structure is a conventional two-span monolithic reinforced concrete structure while the second structure, with almost identical superstructure geometry of the first structure is a composite structure comprised of reinforced concrete, lightweight concrete, and various combinations of fiber reinforced plastic components. Acceleration-time data for the structures were acquired in the field between May 3 – 5, 2001. Next, modal parameters were extracted from the field data. Finite element models of the structures were then developed to aid in the interpretation of the field data. The field data and finite element models were combined to produce more detailed finite element models of the structures. Treating the modal parameters of the updated finite element models and the extracted modal parameters from the field tests as the undamaged and damaged specimens respectively, a nondestructive damage detection of the as-built structures was performed.					
17. KEY WORDS Fiber reinforced polymer composite bridge, system identification, non-destructive damage detection, estimation of structural properties			18. DISTRIBUTION STATEMENT No restrictions. This document is available to the public through the National Technical Information Service, Springfield, VA 22161		
19. SECURITY CLASSIFICATION (of this report) Unclassified		20. NUMBER OF PAGES 58 Pages		21. PRICE	

System Identification and Damage Localization of the  
King Stormwater Channel Bridges  
Based on 3 May 01 Test

FINAL REPORT

Prepared by

N. Stubbs<sup>1</sup>, S. Choi<sup>2</sup>, R.W. Bolton<sup>3</sup>  
Texas Engineering Experiment Station  
College Station, Texas 77843

and

C. Sikorsky<sup>4</sup>

Submitted to:

State of California  
Department of Transportation  
Sacramento, CA 95816

TEES CONTRACT 32525-51640CE

June 2003

- 
1. A.P. and Florence Wiley Professor
  2. Research Associate
  3. Assistant Professor
  4. Senior Bridge Engineer

System Identification and Damage Localization of the  
King Stormwater Channel Bridges  
Based on 3 May 01 Test

FINAL REPORT

Prepared by

N. Stubbs<sup>1</sup>, S. Choi<sup>2</sup>, R.W. Bolton<sup>3</sup>  
Texas Engineering Experiment Station  
College Station, Texas 77843

and

C. Sikorsky<sup>4</sup>

Submitted to:

State of California  
Department of Transportation  
Sacramento, CA 95816

TEES CONTRACT 32525-51640CE

June 2003

- 
1. A.P. and Florence Wiley Professor
  2. Research Associate
  3. Assistant Professor
  4. Senior Bridge Engineer

1. Report No. CA03-0130	2. Government Accession No.	3. Recipient's Catalog No.	
4. Title and Subtitle System Identification and Damage Localization of the Kings Stormwater Channel Bridge		5. Report Date June 2003	6. Performing Organization Code
7. Author(s) Norris Stubbs, Sanghyun Choi, Robert Bolton, Charles Sikorsky		8. Performing Organization Report No.	
9. Performing Organization Name and Address Texas Engineering Experiment Station  Texas A&M University College Station, Texas 77843		10. Work Unit No. (TRAIS)	11. Contract or Grant No. Contract #59A0216
12. Sponsoring Agency Name and Address  California Department of Transportation Division of Engineering Services 1801 30 <sup>th</sup> St., West Building MS-9-2/51 Sacramento, California 95816		13. Type of Report and Period Covered Final Report: June 2000 – March 2003	14. Sponsoring Agency Code
15. Supplementary Notes Prepared in cooperation with the State of California Department of Transportation.			
16. Abstract  The objective of this report is to describe the system identification and nondestructive damage evaluation of two recently constructed bridges in southern California. The first structure is a conventional two-span monolithic reinforced concrete structure while the second structure, with almost identical superstructure geometry of the first structure is a composite structure comprised of reinforced concrete, lightweight concrete, and various combinations of fiber reinforced plastic components. Acceleration-time data for the structures were acquired in the field between May 3 – 5, 2001. Next, modal parameters were extracted from the field data. Finite element models of the structures were then developed to aid in the interpretation of the field data. The field data and finite element models were combined to produce more detailed finite element models of the structures. Treating the modal parameters of the updated finite element models and the extracted modal parameters from the field tests as the undamaged and damaged specimens respectively, a nondestructive damage detection of the as-built structures was performed.			
17. Key Words fiber reinforced polymer composite bridge, system identification, non-destructive damage detection, estimation of structural properties		18. Distribution Statement Unlimited	
19. Security Classification (of this report) Unclassified	20. Security Classification (of this page) Unclassified	21. No. of Pages 54	22. Price

## ABSTRACT

The objective of this report is to describe the system identification and nondestructive damage evaluation of two recently constructed bridges in southern California. The first structure is a conventional two-span monolithic reinforced concrete structure while the second structure, with almost identical superstructure geometry of the first structure, is a composite structure consisting of reinforced concrete, lightweight concrete, and various combinations of fabric reinforced plastics. Acceleration-time data for the structures were acquired in the field between 5/3/01 and 5/5/01. Next, modal parameters were extracted from the field data. Finite element models of the structures were then developed to aid in the interpretation of the field data. The field data and the finite element models were combined to produce more detailed finite element models of the structures. Treating the modal parameters of the updated definite element models and the extracted modal parameters from the field tests as the undamaged and the damaged specimens, respectively, a nondestructive damage detection of the as-built structures was performed.

**DISCLAIMER: The opinions, findings, and conclusions expressed in this publication are those of the authors and not necessarily those of the STATE OF CALIFORNIA**

# TABLE OF CONTENTS

	Page
TABLE OF CONTENTS .....	iii
LIST OF TABLES.....	iv
LIST OF FIGURES .....	v
CHAPTER	
1. INTRODUCTION .....	1
1.1 Overview.....	1
1.2 Objective and Scope of the Report .....	1
1.3 Description and Modal Analysis .....	2
1.4 Approach Used to Meet the Objective.....	2
2. SYSTEM IDENTIFICATION AND NONDESTRUCTIVE DAMAGE DETECTION OF THE REINFORCED CONCRETE (RC) BRIDGE .....	3
2.1 Preliminary Attempt to Model the RC Structure Dynamic Properties via a Finite Element Model.....	3
2.2 Fine-Tuning the RC Finite Element Model Using Field Frequency Data (The Baseline Model).....	4
2.3 As-Built Damage Localization in the RC Bridge Using the Baseline Modal Amplitudes and the Modal Amplitudes Extracted From the Field Data.....	5
3. SYSTEM IDENTIFICATION AND NONDESTRUCTIVE DAMAGE DETECTION OF THE COMPOSITE (FRP) BRIDGE.....	18
3.1 Preliminary Attempt to Model the FRP Structure Dynamic Properties via a Finite Element Model.....	18
3.2 Fine-Tuning the FRP Finite Element Model Using Field Frequency Data (The Baseline Model).....	18
3.3 As-Built Damage Localization in the FRP Bridge Using the Baseline Modal Amplitudes and the Modal Amplitudes Extracted From the Field Data.....	20
4. SUMMARY AND CONCLUSIONS .....	34
REFERENCES .....	35
APPENDICES .....	36
I. System Identification Using Modal Sensitivities and Frequencies .....	36
II. The Damage Index Method .....	40

## LIST OF TABLES

TABLE	Page
2.1	Material Properties of the Initial RC FE Model Subjected to Updating.....8
2.2	MAC Values Among the Field Modes and the Initial RC FE Model .....9
2.3	Comparison Between Frequencies of the Field Modes and the Initial RC FE Model .....9
2.4	Material Properties of the RC FE Model Used for Systems Identification .9
2.5	Comparison Between Frequencies of the Field Modes and the RC FE Model used for Fine-Tuning the FE Model..... 12
2.6	Sensitivity Matrix F for the Kings Stormwater Channel Bridge (RC) .....13
2.7	System Identification for the Kings Stormwater Channel Bridge (RC) ....13
2.8	Identified Material Properties of the Baseline RC Finite Element Structure ..... 13
3.1	Material Properties of the Initial FRP FE Model Subjected to Updating .....22
3.2	MAC Values Among the Field Modes and the Initial FRP FE Model .....24
3.3	Comparison Between Frequencies of the Field Modes and the Initial FE Model.....24
3.4	Material Properties of the FRP FE Model Used for Systems Identification.....24
3.5	Sensitivity Matrix F for the Kings Stormwater Channel Bridge (FRP) ....28
3.6	System Identification for the Kings Stormwater Channel Bridge (FRP) ..28
3.7	Identified Material Properties of the Baseline FRP Finite Element Structure .....28

## LIST OF FIGURES

Figure	Page
2.1 Schematic of FE Model of the RC Bridge.....	8
2.2 Comparison of the Mode Shapes Extracted from Field Data and Mode Shapes Generated from the Initial RC Finite Element Model.....	12
2.3 Sensor Locations for the RC Bridge.....	14
2.4 The Damage Detection Model for the RC Bridge.....	14
2.5 Damage Localization Results using the First Field Bending Mode and the First Baseline Bending Mode of the RC Model.....	15
2.6 Damage Localization Results using the First Torsional Modes From The Field Data and the Baseline RC Model.....	16
2.7 Damage Localization Results using the First Bending and Torsional Modes.....	17
3.1 Schematic of FE Model of the FRP Bridge.....	23
3.2 Comparison of the Mode Shapes Extracted from Field Data and Mode Shapes Generated from the Initial FRP Finite Element Model.....	27
3.3 Sensor Locations for the FRP Bridge.....	29
3.4 The Damage Detection Model for the FRP Bridge.....	29
3.5 Damage Localization Results using the First Field Bending Mode and the First Bending Mode of the Baseline FRP Model.....	31
3.6 Damage Localization Results using the First Torsional Modes From The Field Data and the Baseline FRP Model.....	32
3.7 Damage Localization Results using the First Bending and Torsional Modes.....	33

## 1.0 INTRODUCTION

### 1.1 Overview

In the structural engineering field, for most traditional structures the bulk of the professional effort has focused on the planning, design, fabrication and construction activities. However, for certain special or critical structures, in order to ensure the proper functioning of those structures or to advance the knowledge base of structural engineering, problems that extend beyond the scope of the traditional activities must be considered. For example, the three following problems dealing with model updating, systems identification, and nondestructive damage evaluation have received increasing attention from the technical community in the past two decades. First, given that a finite element model of a particular structure is available in addition to some dynamic response data (such as modal parameters) on the actual structure, how can the knowledge of the field response of the structure be used to increase the accuracy of response prediction of the finite element model? Second, given that a structure has recently been completed in accordance with a set of plans and specifications, to what extent can it be certified that the as-built structure, at least the structural aspects, satisfies the design requirements? Third, and this situation is related to the second issue, given an existing structure for which no data on the pristine structure are available but data are available at some latter date, what are the possible locations of damage in the structure and what are the consequences associated with these flaws?

### 1.2 Objectives and Scope of the Report

This report describes the system identification and the nondestructive damage evaluation of two recently constructed bridges in Southern California. The structures are located on Route 86 in District 08, River County, California. Both structures were completed in 2001. The first structure is a two-span, monolithic, reinforced concrete bridges. The deck spans 60.67 ft., has a width of 42.5 ft., and is 1.42 ft. thick. The substructure consists of two abutments and six equally-spaced circular columns at the center of the bridge. The second bridge is a composite structure with the same geometry as the first bridge. The deck consists of a system of glass fiber reinforced polymer composite deck panels that are supported by six equally-spaced girders. The girders,

which consists of cylindrical carbon shells that are in filled with concrete, are supported by two abutments and a central pier supported by five equally-spaced circular columns.

### **1.3 Description and Modal Analysis**

Single-input, multiple-output (SIMO) vibration tests were performed on both structures between 5/3/01 and 5/5/01. The placement scheme for the accelerometers are shown in Figure 2.3 and Figure 3.3 for the RC bridge and the FRP bridge, respectively. Details of the modal testing procedure and the extraction of modal parameters are discussed elsewhere (see, e.g. Stubbs et al. 1999). Appropriate results of the modal testing are presented in Section 2.2 and Section 3.2 of this report.

### **1.4 Approach Used to Meet Objectives**

The approach to be used here in the analysis of the two bridges can be broken down into four basic stages: (1) the planning and acquisition of acceleration-time data for the structures, (2) the signal processing of that data to yield the modal parameters associated with each structure, (3) the updating of the finite element models of the bridges using the field data, and (4) a nondestructive damage assessment of the as-built structures using the extracted modal parameters from the field data and the numerically generated modal parameters for the updated finite element model of the bridges.

The remainder of this report is organized in three parts. The system identification and nondestructive damage detection of the as-built reinforced concrete bridge is presented in Chapter 2. The system identification and nondestructive damage detection of the as-built composite bridge is presented in Chapter 3. A summary and conclusions section is provided in Chapter 4.

# SYSTEMS IDENTIFICATION AND NONDESTRUCTIVE DAMAGE DETECTION OF THE REINFORCED CONCRETE RC BRIDGE

## 2.1 Preliminary Attempt to Model the RC Structure Dynamic Properties via a Finite Element Model

A schematic of the finite element model of the RC bridge is shown in Figure 2.1. The deck and abutments of the bridge are modeled using plate elements while the railings and columns are modeled using beam elements. Soil-structure interaction is modeled using linear springs. The reinforced concrete is assumed to have a mass density of  $4.70 \text{ lb-sec}^2\text{ft}^{-4}$  and a Poisson's ratio of 0.15. The stiffness properties for the deck, abutments, railings, columns, and the soil are listed in Table 2.1.

A modal analysis was performed on the finite element model using the properties listed in Table 2.1. Modal assurance criteria (MAC) were performed among the first seven numerically generated finite element modes and the first seven modes extracted from the field measurements. The MAC values between the experimental mode shapes and the finite element model proposed in Figure 2.1 are listed in Table 2.2. Note that the MAC values along the diagonal of the table are several orders of magnitude larger than the off-diagonal MAC values. This statement is particularly true for Modes 1,3,5,6, and 7. Eventhough the MAC values between Finite Element Modes 2 and 4 and the Experimental Modes 2 and 4 are somewhat lower, those modes are still the most highly correlated for the two data sets. For convenience, the frequencies extracted from the experimental measurement and the frequencies predicted by the finite element model are listed in Table 2.3. Note that the finite element frequencies are consistently higher than the frequencies derived from field measurements. One explanation of this systematic error may be either an underestimation of certain mass components of the structure or an overestimation of the stiffness components of the structure. A misjudgment in the relative masses or stiffnesses of the components of the model could also lead to a discrepancy between the two data sets. Figure 2.2 provides a visual comparison of the mode shapes extracted from the field data and the mode shapes generated from the finite element model. From a visual comparison of these mode shapes, the two systems appear to be highly correlated.

## 2.2 Fine-Tuning the RC Finite Element Model using Field Frequency Data (The Baseline Model)

After analyzing the relative frequencies between the finite element predictions and the field experiment, a closer examination of the as-built plans of the bridge suggested that a more realistic set of stiffness properties for the bridge superstructure and substructure might be provided by the values presented in Table 2.4. Essentially, a single modification was made to the model; namely, the effective elastic modulus of the deck and the columns were increased from 3,400 ksi to approximately 4,540 ksi. Note that the stiffness properties of the railings and the soil-structure interaction remained essentially unchanged. The results of the dynamic analysis are presented in Table 2.5. Note that while the trend in the predictions using these properties do not show the obvious systematic error as those presented in Table 2.3, the error between measured and predicted frequencies has been significantly reduced (compare Column 4 of Table 2.3 with Column 4 of Table 2.5). We also wish to indicate that Modes 2 and 4 have been eliminated because of the low MAC values between the modes obtained from the finite element analysis and the field data.

In the model to be updated, the following three parameters were taken as unknowns: the effective modulus of the deck and abutments, the effective modulus of the columns, and the effective modulus of the railings. Thus the sensitivity matrix is a 5x3 matrix, since five frequencies were used. Recall that the stiffness-frequency sensitivity matrix relates fractional changes in parameter stiffnesses to changes in fractional eigenvalues. Note that in the model it is assumed that moduli of subgrade reaction for the abutments and columns (which were based on geotechnical information provided on the plans for the structure), and the mass density of the concrete are assumed to be known with relatively greater confidence. The sensitivity matrix for the given system are given in Table 2.6. As physically expected, the deck and abutment subsystems, mostly the deck, dominate the sensitivity distribution.

The results of the iteration process described in the appendices are summarized in Table 2.7. Note that the system converged in four iterations. The calculated frequencies for the finite element model and those from the bridge are listed, respectively, in Column 2 and Column 6 of the table. The percentage errors for each mode of the initial finite

element model and the fine-tuned (updated) models are shown in the last column of Table 2.7. The percentage error in frequencies between the initial finite element model and the real bridge ranged from 2.41 to 5.52 percent. The same measures for the updated finite element ranged from 0.02 to 2.59 percent.

Using the updating procedure described in the appendices, the updated moduli for the deck and abutments, columns, and railings are listed in Table 2.8. The general trend in comparing Table 2.4 and Table 2.8 is the reduction in the moduli of the initial finite element model and the updated finite element model. These observations are consistent with the frequencies for the initial finite element model and the frequencies for the actual structure presented in Table 2.5. The structure with the properties indicated in Table 2.5 is also referred to as the “baseline” structure. The modal frequencies of this structure are close to the real structure and the mode shapes of the structure are those of an ideal structure with no flaws.

### **2.3 As-Built Damage Localization in the RC Bridge Using the Baseline Modal Amplitudes and the Modal Amplitudes Extracted From the Field Data**

In Section 2.2, frequency information was used to generate a flawless baseline model of the bridge. That structure has eigenfrequencies that are very close to those of the actual structure ( $0 \leq 2.6\%$ ). In order to detect possible flaws in the as-built structure, we propose to use the Damage Index Method in which the modal amplitudes of the baseline structure are taken as the undamaged mode shapes and the mode shapes extracted from the 3 May 2001 field test represent the potentially damaged structure.

The layout for four lines of accelerometers the structure is shown in Figure 2.3. The longitudinal and transverse spacing of the sensors are 9.83 ft. and 13.00 ft., respectively. Using the measured modal amplitudes as a reference, cubic splines are generated between the first and last sensor along each line. Next a damage detection model is defined such that each element has a length of 1.2917 feet in the longitudinal direction. Thus there are 48 elements along each sensor line and a total of 192 (48x4) elements in the model. The damage detection model is shown in Figure 2.4.

Damage localization results were generated for two modes. The first bending Mode (Mode 1, Figure 2.2) and the first torsional Mode (Mode 3, Figure 2.2). These two modes were selected because of the high MAC values between the field modes and the

finite element modes. The normalized damage indicator for the 192 elements are shown in Figure 2.5. Note that only the first bending modes (Figure 2.3 and Figure 2.3b) were used in the analysis. Damage localization results for the elements along Sensor Line A1-A7 are shown in Figure 2.5a. A damage threshold of one was selected to indicate the possible location of damage. If the damage indicator exceeds one, then damage is assumed to exist. Note that setting the threshold at this low value is very conservative and may lead to false positive predictions. However these predictions should be confirmed with visual inspection or other local methods. On the basis of the results presented in Figure 2.3a, we conclude that there are no as-built flaws along Sensor Line A1-A7.

From Figure 2.5b we conclude that as-built flaws may exist along two regions of Sensor Line B1-B7. The first region includes Elements 23-25 which defines a 3.86 ft. interval beginning 28.42 ft. from Sensor B1. The second region includes Elements 32-34 which defines a 3.86 ft. interval beginning 40.04 ft. from Sensor B1.

From Figure 2.5c we conclude that as-built flaws may exist along two regions of Sensor Line C1-C7. The first region includes Elements 6-9 which defines a 5.17 ft. interval beginning 6.46 ft. from Sensor C1. The second region includes Elements 24-25 which defines a 2.58 ft. interval beginning 29.71 ft. from Sensor C1.

Finally, from Figure 2.5d as-built flaws may again exist in two regions. The first region includes Elements 14-17 which includes a 5.17 ft. interval beginning 16.79 ft. from sensor D1. The second region includes Elements 23-25 which defines a 3.86 ft. interval beginning 28.42 ft. from Sensor D1.

The damage localization results using the first torsional mode are presented in Figure 2.6. Note that only one set of elements are presented in this figure as compared to the four lines presented for the latter bending case. The reason for having only one line for the torsional case is that in the development of the torsional strain energy for the deck, the entire cross section must be considered in developing the angle of twist for each element. So in effect, if a torsional mode is used the damage detection model reduces to 48 elements each with a length of 1.2917 feet and a width equal to the width of the bridge. From Figure 2.6, damage localization using the first torsional mode suggests that

damage may exist in the region occupied by Elements 25 to 31 which corresponds to an 9.04 ft. interval located 31.00 ft. from Sensors A1 to D1.

A pictorial representation of the possible damage distribution on the deck is presented in Figure 2.6. The bending mode predicts damage in two distinct regions in the south span, one distinct region in the north span, and along a strip near the centerline of the bridge. The torsional mode predicts damage in a strip near the centerline of the bridge.

**Table 2.1 Material Properties of the Initial RC FE Model Subjected to Updating**

Elements	Properties	
Deck,	Mass Density	4.70 lb sec <sup>2</sup> /ft <sup>4</sup>
Column, Abutment	Poisson's Ratio	0.15
And Railings	Elastic Modulus	3,400 ksi
Soil	Modulus of Subgrade	8,000 kcf (Vertical)
	Reaction	800 kcf (Lateral)

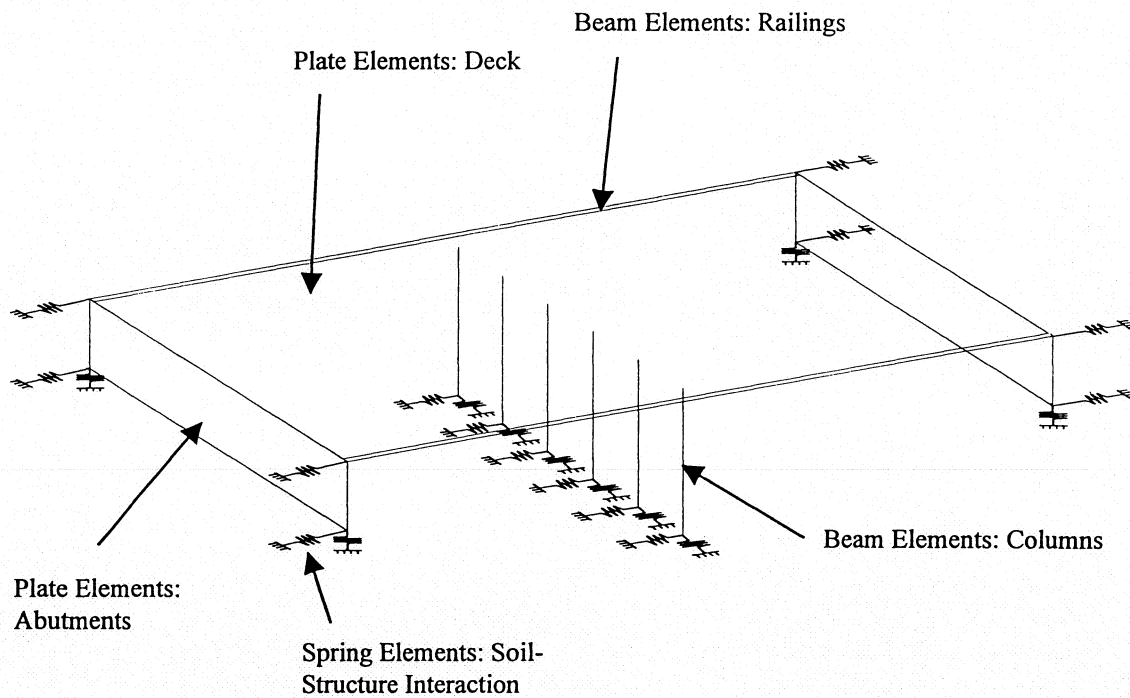


**Figure 2.1 Schematic of FE Model of the RC Bridge**

**Table 2.2 MAC Values Among the Field Modes and the Initial RC FE Model**

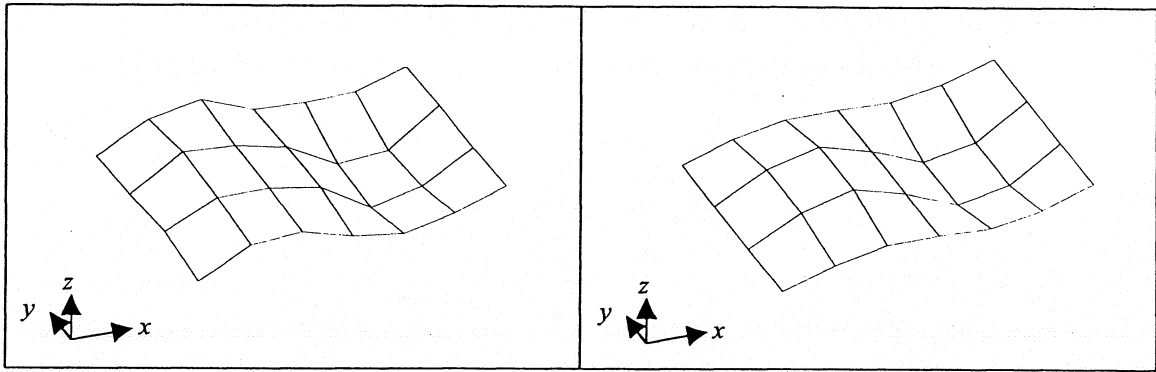
		1/EX	2/EX	3/EX	4/EX	5/EX	6/EX	7/EX
		11.244	13.564	16.412	19.481	21.745	23.312	35.375
1/FE	13.208	0.929	0.201	0.001	0.000	0.000	0.017	0.000
2/FE	16.683	0.001	0.663	0.004	0.091	0.004	0.000	0.001
3/FE	18.974	0.001	0.018	0.982	0.198	0.000	0.000	0.038
4/FE	21.136	0.000	0.030	0.003	0.668	0.014	0.000	0.000
5/FE	25.094	0.011	0.042	0.000	0.000	0.895	0.011	0.001
6/FE	26.509	0.036	0.001	0.000	0.000	0.052	0.977	0.000
7/FE	40.622	0.000	0.000	0.079	0.012	0.004	0.000	0.982

**Table 2.3 Comparison Between Frequencies of the Field Modes and the Initial RC FE Model**

Mode Number	Frequency (Hz)		
	Field	Initial FE Model	Error(%)
1	11.244	13.208	
2	13.564	16.683	
3	16.412	18.974	
4	19.481	21.136	
5	21.745	25.094	
6	23.312	26.509	
7	35.375	40.622	

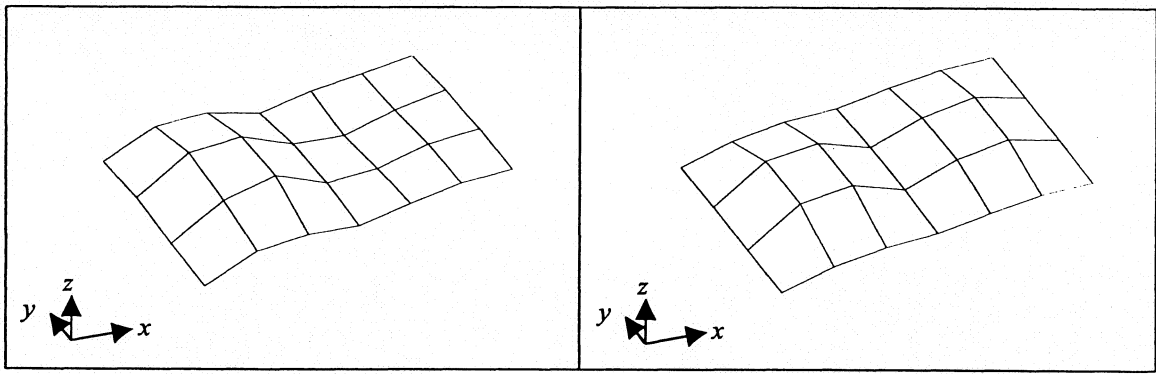
**Table 2.4 Material Properties of the RC FE Model Used for System Identification**

	Deck and Abutments	Column	Railings	Modulus of Subgrade Reaction		
				Abutment Vertical	Abutment Lateral	Column Lateral
E (ksi)	4,543	4,538	3,400			
k (kcf)				8,009	8,034	800



(a) Experimental Mode 1 at 11.244 Hz

(b) Initial FE Mode 1 at 12.951 Hz

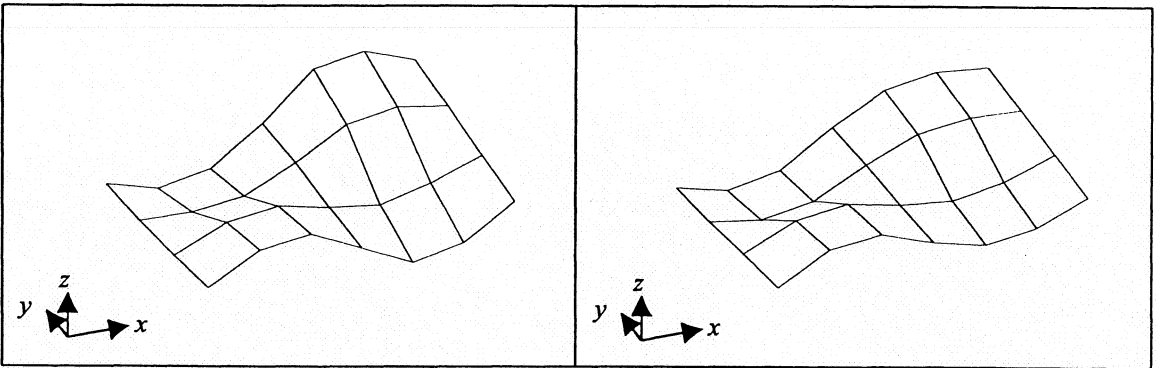


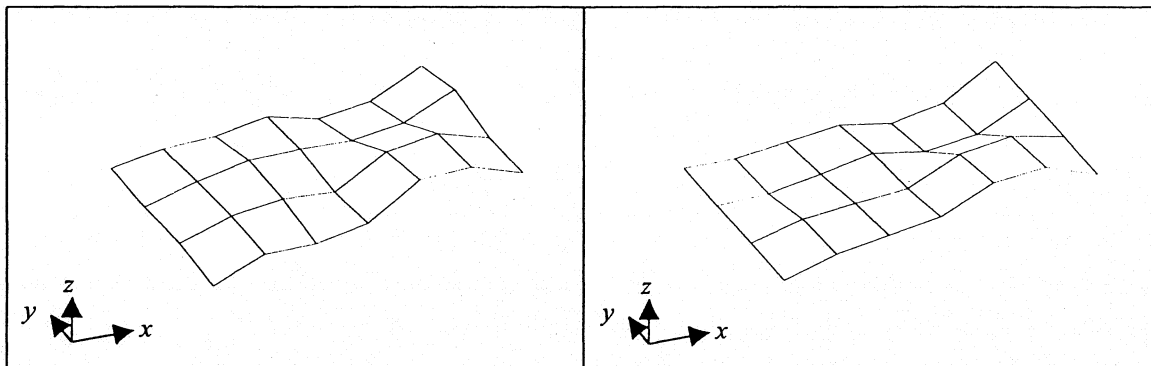
(c) Experimental Mode 2 at 13.564 Hz

(d) Initial FE Mode 2 at 15.836 Hz

(e) Experimental Mode 3 at 16.412 Hz

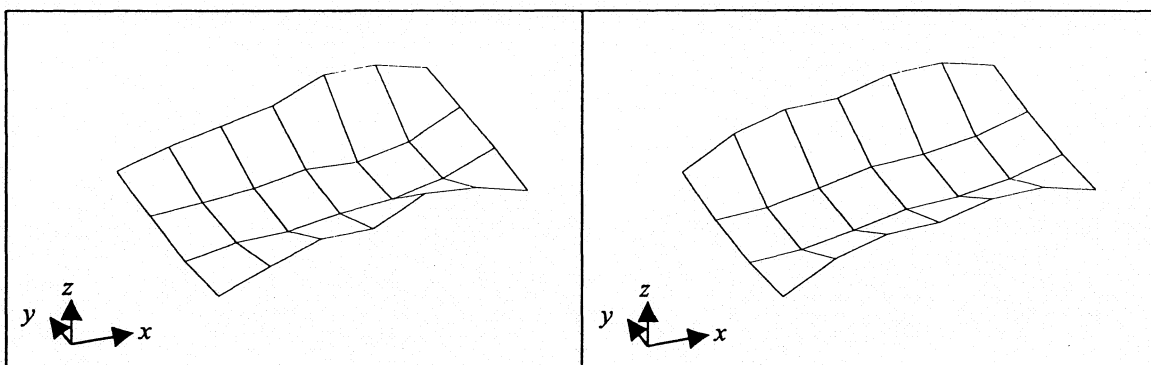
(f) Initial FE Mode 3 at 17.579 Hz



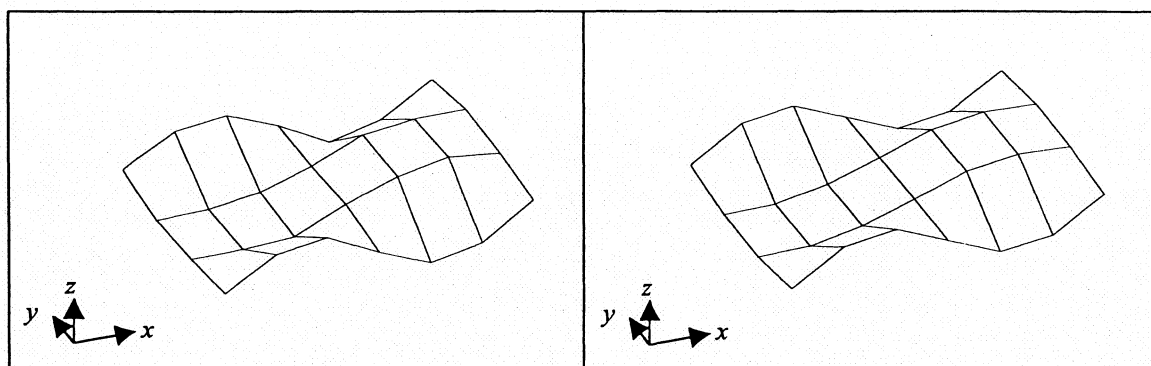


(g) Experimental Mode 4 at 19.481 Hz

(h) Initial FE Mode 4 at 19.309



Hz

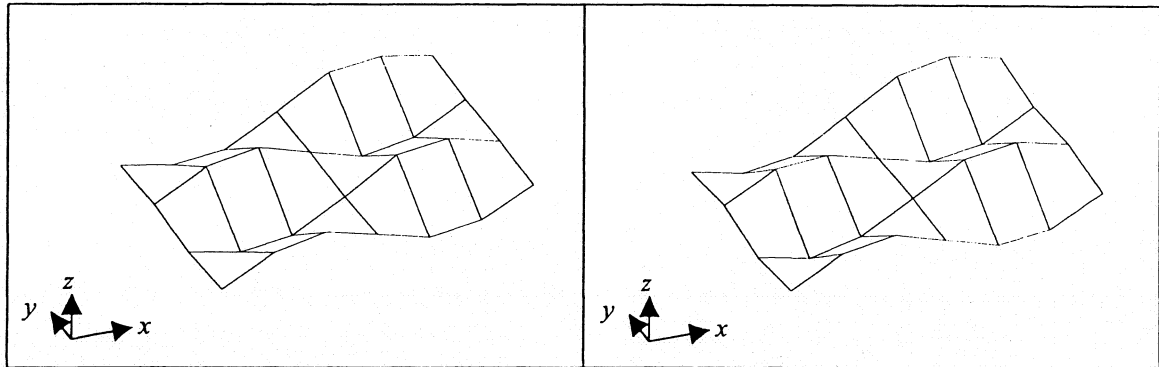


(i) Experimental Mode 5 at 21.745 Hz

(j) Initial FE Mode 5 at 22.998 Hz

(k) Experimental Mode 6 at 23.312 Hz

(l) Initial FE Mode 6 at 25.189 Hz



(m) Experimental Mode 7 at 35.375 Hz

(n) Initial FE Mode 7 at 36.972 Hz

**Figure 2.2 Comparison of Mode Shapes Extracted from Field Data and Mode Shapes Generated from the Initial RC Finite Element Model**

**Table 2.5 Comparison Between Frequencies of the Field Modes and the RC FE Model used for Fine-Tuning the FE Model**

Mode Number	Frequency (Hz)		
	Field	Initial FE Model for Updating	Percent Error
1	11.244	11.865	5.52
3	16.412	15.634	4.74
5	21.745	22.864	5.15
6	23.312	22.750	2.41
7	35.375	34.600	4.42

**Table 2.6 Sensitivity Matrix F for the Kings Stormwater Channel Bridge (RC)**

Mode	Deck & Abutments	Columns	Railings
1	0.7328	0.0286	0.1795
3	0.6628	0.0153	0.3059
5	0.6165	0.2529	0.1534
6	0.7688	0.0062	0.2186
7	0.8682	0.0027	0.1301

**Table 2.7 System Identification for the Kings Stormwater Channel Bridge (RC)**

Mode (Exp.)	Frequency of Initial FE model*	Updated Frequencies (Hz)			Frequency of Target Structure	Error (%)	
		Iter.1	Iter.3	Iter.4		Initial	Final
1	11.865	11.334	11.536	11.535	11.244	5.52	2.59
3	15.634	15.917	16.417	16.416	16.412	4.74	0.02
5	22.864	20.972	21.696	21.693	21.745	5.15	0.24
6	22.750	22.357	22.952	22.950	23.312	2.41	1.55
7	36.939	34.600	35.185	35.183	35.375	4.42	0.54

**Table 2.8 Identified Material Properties of the Baseline RC Finite Element Structure**

	Deck and Abutments	Column	Railings	Modulus of Subgrade Reaction		
				Abutment Vertical	Abutment Lateral	Column Lateral
E (ksi)	3,439	3,354	2,449			
k (kcf)				8,009	8,034	800

	D1	D2	D3	D4	D5	D6	D7
	C1	C2	C3	C4	C5	C6	C7
	B1	B2	B3	B4	B5	B6	B7
	A1	A2	A3	A4	A5	A6	A7



**Figure 2.3 Sensor Locations for the RC Bridge**

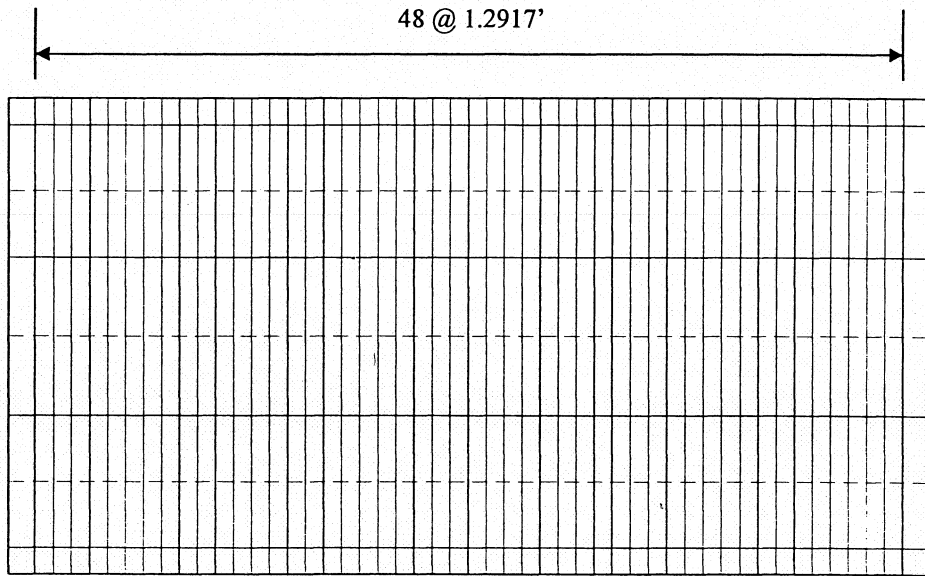
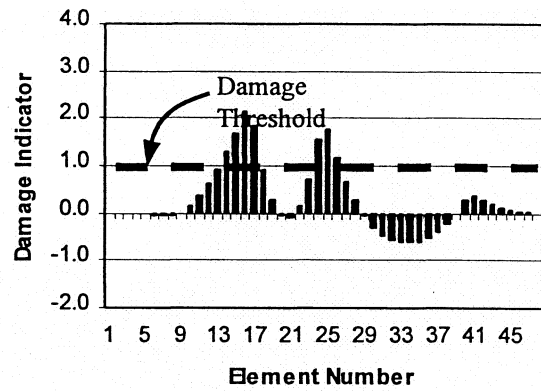
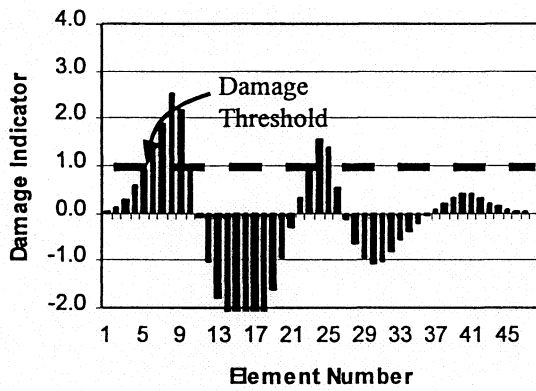
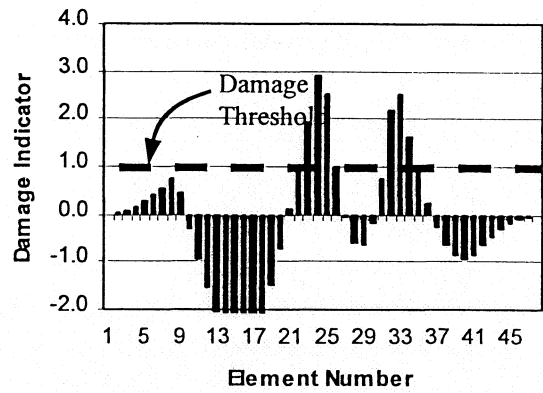
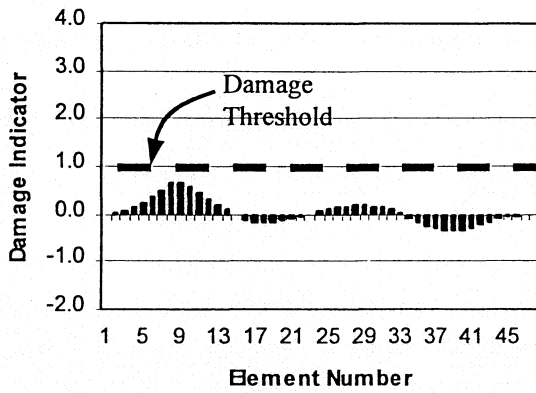


**Figure 2.4 The Damage Detection Model for the RC Bridge**



(a)

(b)

(c)

(d)

**Figure 2.5 Damage Localization Results using the First Field Bending Mode and the First Baseline Model Bending Mode of the RC Model: (a) Result using the Measurement along the Sensors A1 - A7; (b) Result using the Measurement along the Sensors B1 - B7 ; (c) Result using the Measurement along the Sensors C1 - C7; (d) Result using the Measurement along the Sensors D1 - D7**

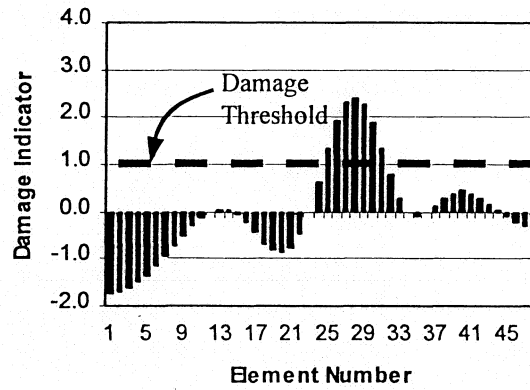


**Figure 2.6 Damage Localization Results using the First Torsional Modes from the Field Data and the Baseline RC Model**

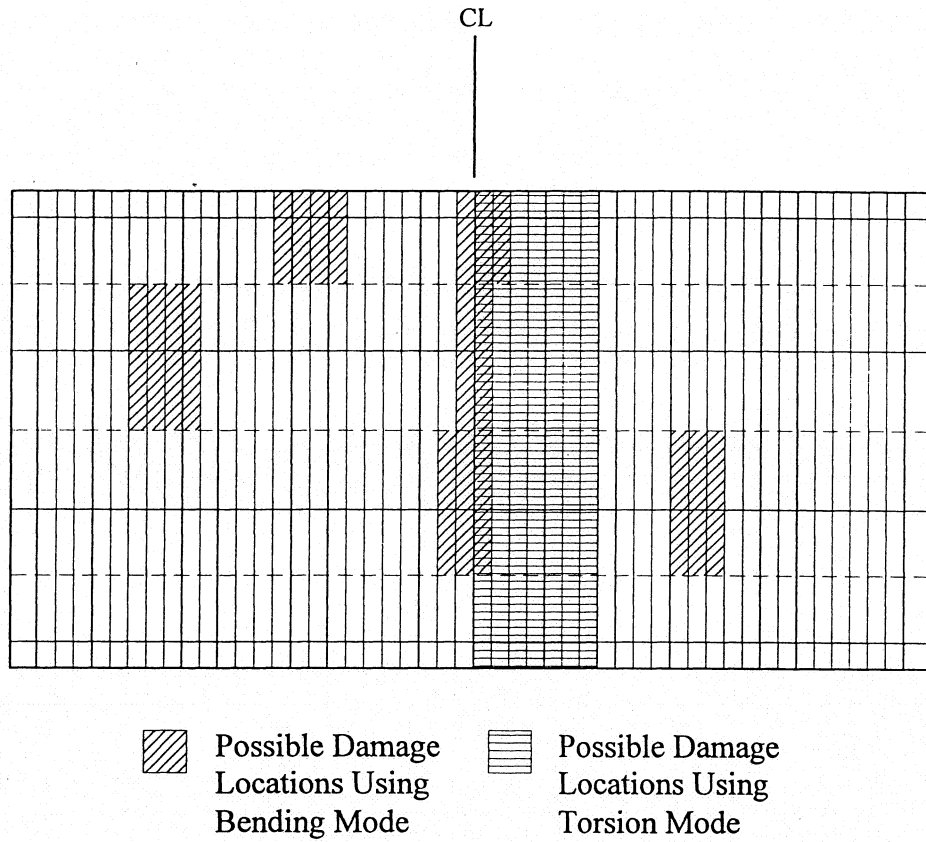


**Figure 2.7 Damage Localization Results using the First Bending and Torsional Modes**

### **3.0 SYSTEM IDENTIFICATION AND NONDESTRUCTIVE DAMAGE DETECTION OF THE COMPOSITE (FRP) BRIDGE**

#### **3.1 Preliminary Attempt to Model the FRP Structure Dynamic Properties via a Finite Element Model**

A schematic of the finite element model of the composite bridge is shown in Figure 3.1. The deck of the bridge is modeled using plate elements while the railings and columns are modeled using beam elements. Soil-structure interaction is modeled using linear springs. The abutments and the cap beam are modeled using brick elements. The reinforced concrete of the columns and abutments is assumed to have a mass density of  $4.70 \text{ lb-sec}^2 \text{ ft}^{-4}$  and the mass density of the girders is assumed to have a value of  $4.8 \text{ lb-sec}^2 \text{ ft}^{-4}$ . Poisson's ratio for all concrete is assumed to be 0.15. The stiffness properties for the deck, abutments, railings, columns, and the soil are listed in Table 3.1.

A modal analysis was performed on the finite element model using the properties listed in Table 3.1. Modal assurance criteria (MAC) were performed among the first eight numerically generated finite element modes and the first eight modes extracted from the field measurements. The MAC values between the experimental mode shapes and the finite element model proposed in Figure 3.1 are listed in Table 3.2. Again as for the RC bridge, note that the MAC values along the diagonal of the table are orders of magnitude larger than the off-diagonal MAC values (except for Modes 4,5, and 7). This statement is particularly true for Modes 1,2,3, and 6. For convenience, the frequencies extracted from the experimental measurement and the frequencies predicted by the finite element model are listed in Table 3.3. Note again that the finite element frequencies are consistently higher than the frequencies derived from field measurements. Figure 3.2 provides a visual comparison of the mode shapes extracted from the experimental data and the mode shapes generated from the finite element model. From a visual comparison of these mode shapes, the two systems again appear to be highly correlated.

#### **3.2 Fine-Tuning the FRP Finite Element Model Using Field Frequency Data (The Baseline Structure)**

The set of stiffness and mass properties for the bridge superstructure and substructure are presented in Table 3.4. Note that the stiffness properties of the railings

and the soil-structure interaction are assumed to remain unchanged with respect to the RC bridge.

In the model to be updated, the following five parameters were taken as unknowns: the effective modulus of the deck, the effective modulus of the girders, the effective modulus of the railings, and the mass densities of the deck and girders. Thus the sensitivity matrix is a 6x5 matrix, since six frequencies were used. Modes 4 and 8 in Table 3.2 were omitted because of the relatively low MAC values between the finite element model and the experimental results. Recall that the stiffness-frequency sensitivity matrix relates fractional changes in parameter stiffnesses to changes in fractional eigenvalues and that the mass-frequency sensitivity matrix relates fractional changes in parameter masses to changes in fractional eigenvalues.. Note that as in the previous problem with the RC bridge, in this model it is assumed that moduli of subgrade reaction for the abutments and columns, and the mass density of the concrete are known. The elements of the sensitivity matrix for the given structural model are given in Table 3.5. As physically expected, the deck-girder system, dominates the sensitivity distribution.

The results of the iteration process described in the appendices are summarized in Table 3.6. Note that the system converged in three iterations. The calculated frequencies for the finite element model and those from the bridge are listed, respectively, in Column 2 and Column 6 of the table. The percentage error for each mode for the initial finite element model and the fine-tuned (updated) models are shown in the last column of Table 3.6. The percentage error in frequencies between the initial finite element model and the bridge ranged from 2.94 to 14.9. The same measures for the updated finite element ranged from 1.99 to 5.32 percent.

Using the updating procedure described in the appendices, the updated moduli for the deck, girders, railings and the mass densities of the deck and girders are listed in Table 3.7. The general trend in comparing Table 3.4 and Table 3.7 is the reduction in the moduli of the initial finite element model and the updated finite element model. These observations are consistent with the frequencies for the initial finite element model and the frequencies for the actual structure presented in Table 3.6. Again the structure with the properties indicated in Table 3.7 is referred to as the “baseline” structure. As stated

previously, the modal frequencies of this structure are close to the real structure and the mode shapes of the structure are those of an ideal structure with no flaws.

### **3.3 As-Built Damage Localization in the FRP Bridge Using the Baseline Modal Amplitudes and the Modal Amplitudes Extracted From the Field Data**

In Section 3.2, frequency information was used to generate a flawless baseline model of the composite bridge. The baseline structure has eigenfrequencies that are very close to those of the actual structure (with an error between 1.02 and 5.32 percent). In order to detect possible flaws in the as-built structure tested on 5/3/2001, we again propose to use the Damage Index Method in which the modal amplitudes of the baseline structure are taken as the undamaged mode shapes and the mode shapes extracted from the 5/3/2001 field test represent the potentially damaged structure.

The layout for six lines of accelerometers the structure is shown in Figure 3.3. The longitudinal and transverse spacing of the sensors are 9.83 ft. and approximately 8 ft., respectively. Using the measured modal amplitudes as a reference, cubic splines are generated between the first and last sensor along each line. Next a damage detection model is defined such that each element has a length of 1.2917 feet in the longitudinal direction. Thus there are 48 elements along each sensor line and a total of 288 elements in the model. The damage detection model is shown in Figure 3.4.

Damage localization results were generated for two modes. The first bending mode (Mode 1, Figure 3.2), and the first torsional Mode (Mode 3, Figure 3.2). Again, these two modes were selected because of the high MAC values between the field modes and the finite element modes. The normalized damage indicator for the 288 elements are shown in Figure 3.5. Note that only the first bending modes (Figure 3.2a and Figure 3.2) were used in the analysis. Damage localization results for the elements along Sensor Line A1-A7 are shown in Figure 3.5a. A damage threshold of one was again selected to indicate the possible location of damage. On the basis of the results presented in Figure 3.5a, we conclude that there are no as-built flaws along Sensor Line A1-A7.

From Figure 3.5b we also conclude that there are no as-built flaws along Sensor Line B1-B7.

From Figure 3.5c we conclude that as-built flaws may exist along two regions of Sensor Line C1-C7. The first region includes Element 8 which defines a 1.2917 ft.

interval beginning 9.04 ft. from Sensor C1. The second region includes Elements 39-43 which defines a 6.46 ft. interval beginning 49.08 ft. from Sensor C1.

From Figure 3.5d as-built flaws may again exist in two regions. The first region includes Elements 8-10 which includes a 3.89 ft. interval beginning 9.04 ft. from sensor D1. The second region includes Elements 38-43 which defines a 7.75 ft. interval beginning 47.8 ft. from Sensor D1.

From Figure 5e, we conclude that as-built flaws may exist along two regions of Sensor line E1-E7. The first region includes Elements 7-12 which defines a 7.75 ft. interval beginning 7.75 ft. from Sensor E1. The second region includes Elements 7.75 which defines a 7.75 ft. interval beginning 47.79 ft. from Sensor E1.

From Figure 3.5f, we conclude that there are no as-built flaws along Sensor line F1-F7.

The damage localization results using the first torsional mode are presented in Figure 3.6. Again note that only one set of elements are presented in this figure as compared to the six lines presented for the latter bending case. Just to remind the reader, the reason for having only one line for the torsional case is that in the development of the torsional strain energy for the deck, the entire cross section must be considered in developing the angle of twist for each element. So in effect, if a torsional mode is used, the damage detection model reduces to 48 elements each with a length of 1.2917 feet and a width equal to the width of the bridge. From Figure 3.6, damage localization using the first torsional mode suggests that damage may exist in the region occupied by Elements 18 to 24 which corresponds to an 9.04 ft. interval located 21.96 ft. from Sensors A1 to D1. A pictorial representation of the possible damage on the deck is presented in Figure 3.7.

**Table 3.1 Material Properties of the Initial FRP FE Model Subjected to Updating**

Elements	Properties		
Deck	Mass Density	2.82	lb sec <sup>2</sup> /ft <sup>4</sup>
	Poisson's Ratio	0.175	
	Elastic Modulus	1,800	ksi
Girders	Mass Density	4.80	lb sec <sup>2</sup> /ft <sup>4</sup>
	Poisson's Ratio	0.15	
	Elastic Modulus	3,000	ksi
Column	Mass Density	4.70	lb sec <sup>2</sup> /ft <sup>4</sup>
	Poisson's Ratio	0.15	
	Elastic Modulus	3,354	ksi
Abutments and Cap Beam	Mass Density	4.70	lb sec <sup>2</sup> /ft <sup>4</sup>
	Poisson's Ratio	0.15	
	Elastic Modulus	3,439	ksi
Modulus of Subgrade Reaction	Abutment Vertical	8009	kcf
	Abutment Lateral	8034	kcf
	Column Lateral	800	kcf

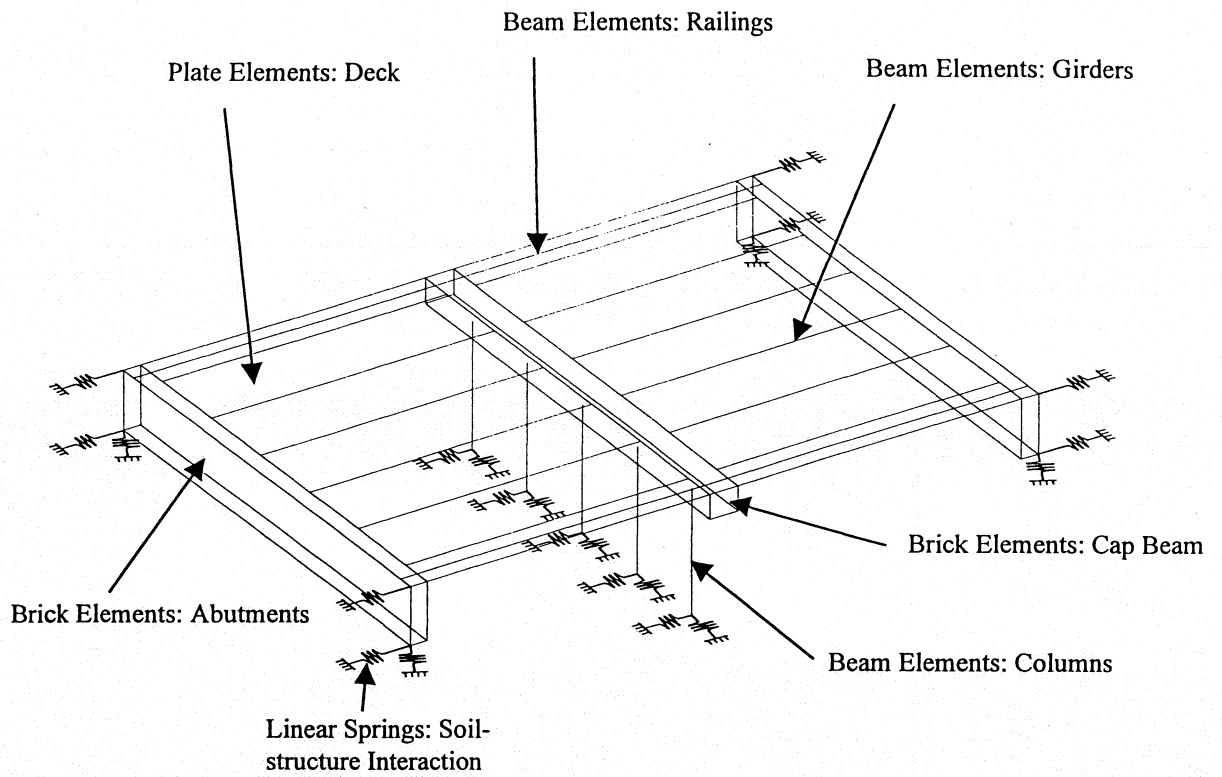


**Figure 3.1 Schematic of FE Model of the FRP Bridge**

**Table 3.2 MAC Values Among the Field Modes and the Initial FRP FE Model**

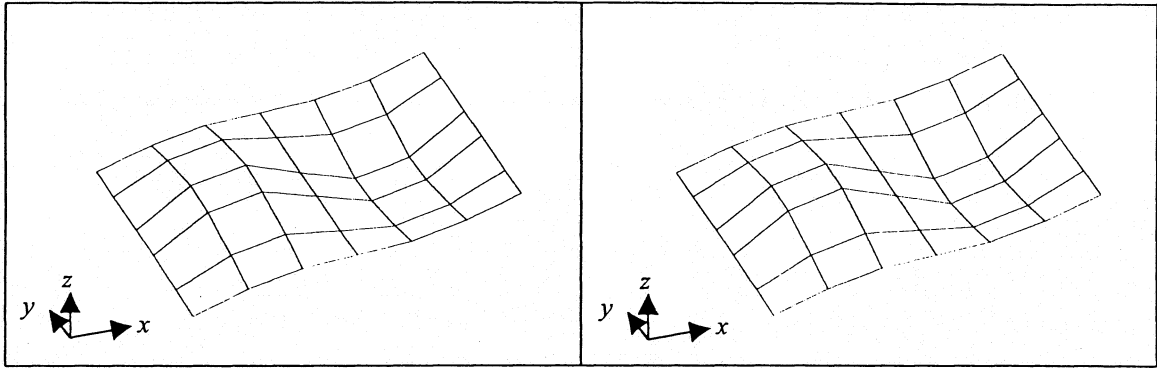
		1/EX	2/EX	3/EX	4/EX	5/EX	6/EX	7/EX	8/EX
		11.033	13.110	15.360	16.921	19.005	25.585	26.390	34.941
1/FE	12.145	0.993	0.022	0.000	0.000	0.000	0.000	0.005	0.000
2/FE	15.058	0.000	0.925	0.005	0.006	0.003	0.018	0.000	0.001
3/FE	15.912	0.002	0.033	0.990	0.000	0.017	0.000	0.000	0.051
4/FE	17.697	0.000	0.012	0.000	0.539	0.152	0.000	0.000	0.000
5/FE	19.912	0.001	0.000	0.000	0.255	0.759	0.005	0.571	0.004
6/FE	26.336	0.000	0.009	0.001	0.034	0.004	0.946	0.000	0.001
7/FE	29.773	0.002	0.000	0.000	0.034	0.085	0.006	0.862	0.001
8/FE	40.854	0.000	0.006	0.121	0.000	0.002	0.000	0.000	0.725

**Table 3.3 Comparison Between Frequencies of the Field Modes and the Initial FE Model**

Mode Number	Frequency (Hz)	
	Experiment	Initial FE Model
1	11.033	12.145
2	13.110	15.058
3	15.360	15.912
4	16.921	17.697
5	19.005	19.912
6	25.585	26.336
7	26.390	29.773
8	34.941	40.854
9	35.833	-

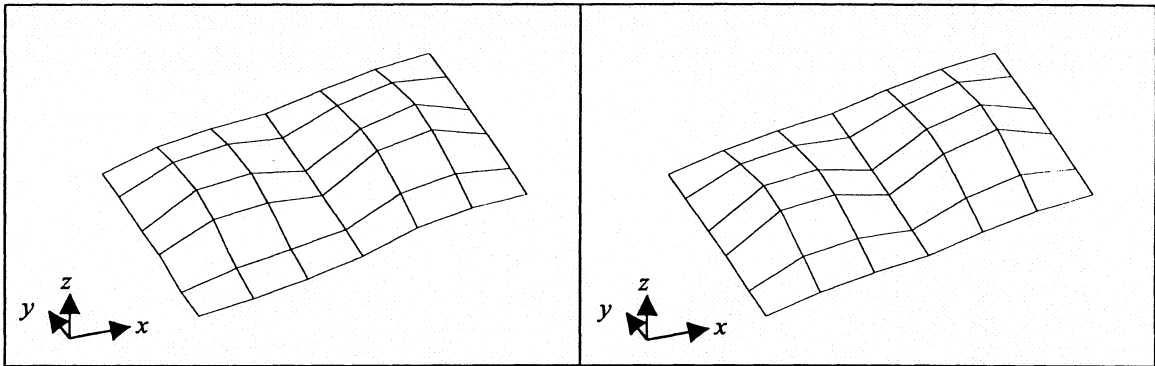
**Table 3.4 Material Properties of the FRP FE Model Used for Systems Identification**

	Deck		Girder		Railings
	Stiffness	Mass	Stiffness	Mass	Stiffness
E (ksi)	1,800		3,000		2,449
$\rho$ (lb sec <sup>2</sup> /ft <sup>4</sup> )		2.82		4.8	



(a) Experimental Mode 1 at 11.033 Hz

(b) Initial FE Mode 1 at 12.145 Hz

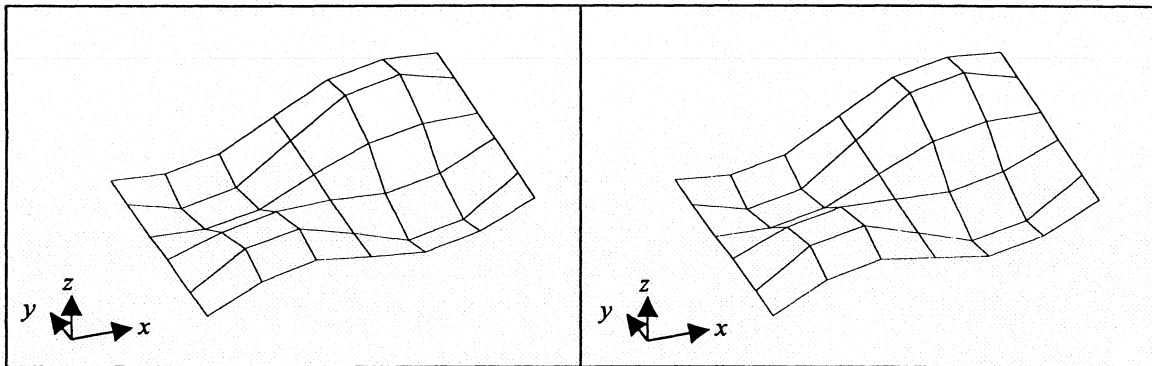


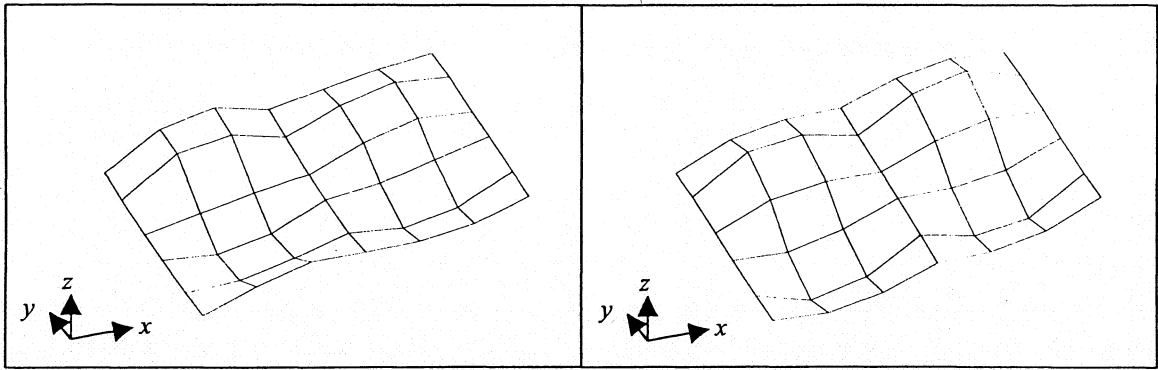
(c) Experimental Mode 2 at 13.110 Hz

(d) Initial FE Mode 2 at 15.058 Hz

(e) Experimental Mode 3 at 15.360 Hz

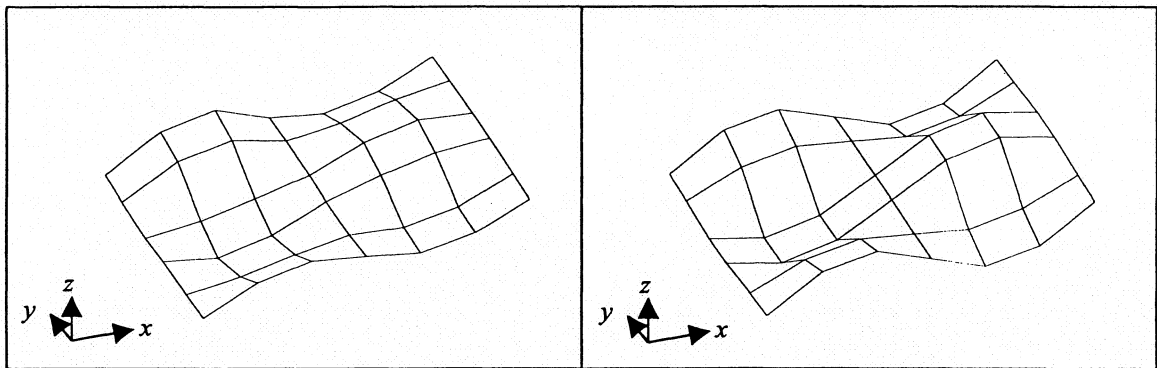
(f) Initial FE Mode 3 at 15.912 Hz





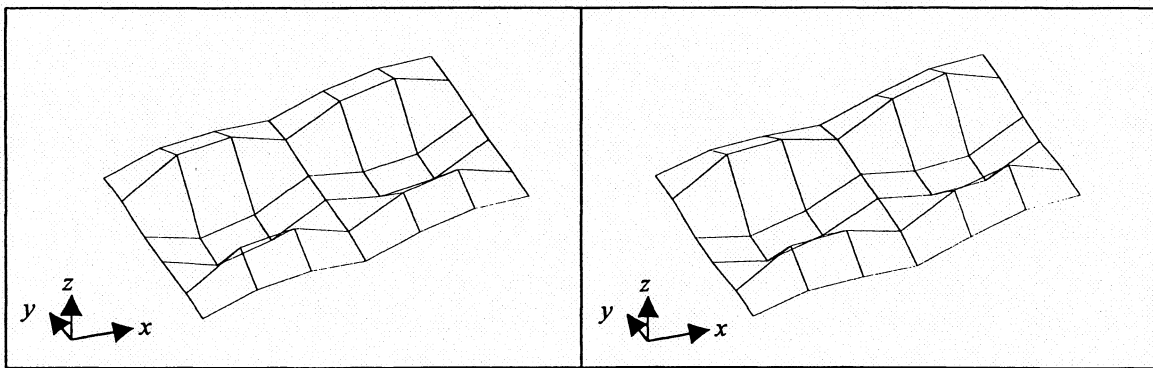
(g) Experimental Mode 4 at 16.921 Hz

(h) Initial FE Mode 4 at 17.697 Hz



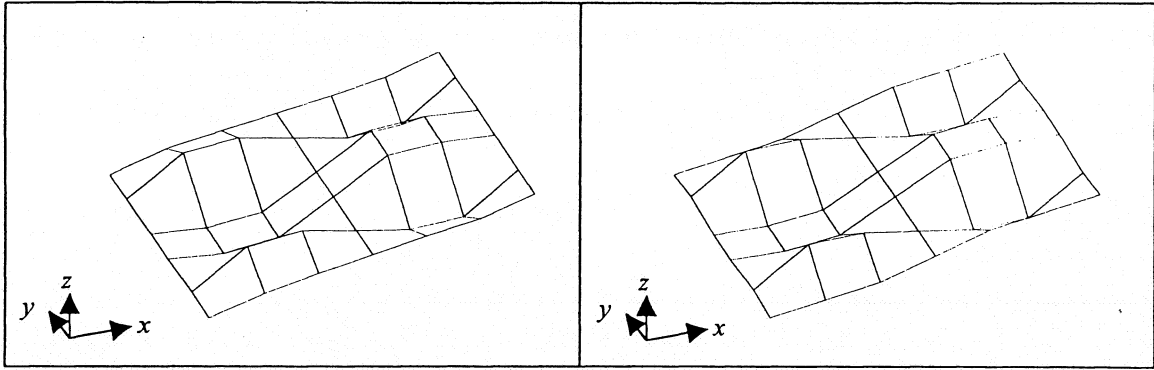
(i) Experimental Mode 5 at 19.005 Hz

(j) Initial FE Mode 5 at 19.912 Hz



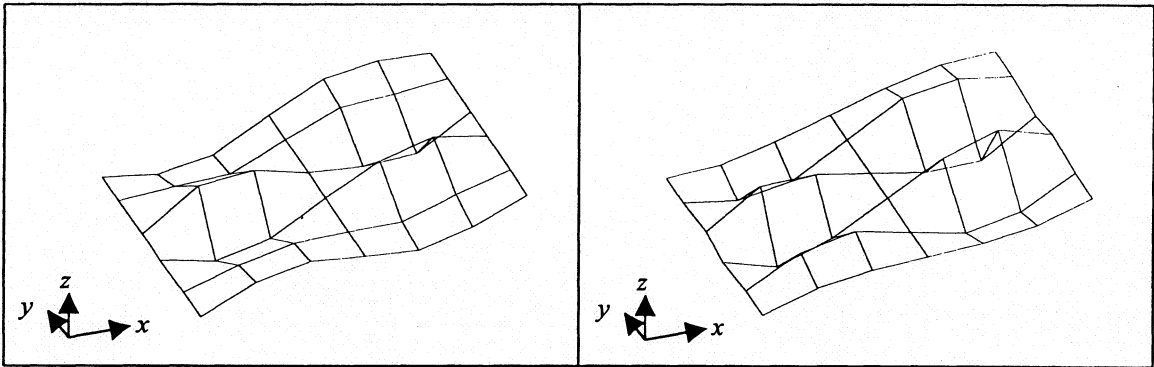
(k) Experimental Mode 5 at 25.585 Hz

(l) Initial FE Mode 5 at 26.336 Hz



(m) Experimental Mode 7 at 26.390 Hz

(n) Initial FE Mode 7 at 29.773 Hz



(o) Experimental Mode 8 at 34.941 Hz

(p) Initial FE Mode 8 at 40.854 Hz

**Figure 3.2 Comparison of the Mode Shapes Extracted From Field Data and Mode Shapes Generated From the Initial FRP Finite FRP Element Model**

**Table 3.5 Sensitivity Matrix F for the Kings Stormwater Channel Bridge (FRP)**

Mode	Group 1	Group 2	Group 3	Group 4	Group 5
	Deck Stiffness	Girder Stiffness	Deck Mass	Girder Mass	Railings Stiffness
1	0.3153	0.4590	-0.6701	-0.2569	0.0658
2	0.3215	0.4867	-0.6775	-0.2586	0.0080
3	0.3377	0.2981	-0.6271	-0.2486	0.2175
5	0.2535	0.1720	-0.5116	-0.2108	0.3958
6	0.5718	0.1641	-0.4831	-0.2047	0.0410
7	0.5504	0.1366	-0.5001	-0.2284	0.2111

**Table 3.6 System Identification for the Kings Stormwater Channel Bridge (FRP)**

Mode	Frequency of Initial FE model*	Updated Frequencies (Hz)			Frequency of Target Structure	Error (%)	
		Iter. 1	Iter. 2	Iter. 3		Initial	Final
1	12.145	11.214	11.144	11.145	11.033	10.1	1.02
2	15.058	13.892	13.805	13.807	13.110	14.9	5.32
3	15.912	14.763	14.675	14.677	15.360	3.59	4.45
5	19.912	18.717	18.625	18.627	19.005	4.77	1.99
6	26.336	24.647	24.524	24.527	25.585	2.94	4.14
7	29.773	27.764	27.614	27.617	26.390	12.8	4.65

**Table 3.7 Identified Material Properties of the Baseline FRP Finite Element Structure**

	Deck		Girder		Railings
	Stiffness	Mass	Stiffness	Mass	Stiffness
E(ksi)	1,636		2,790		2,364
$\rho$ (lb sec <sup>2</sup> /ft <sup>4</sup> )		3.21		5.07	

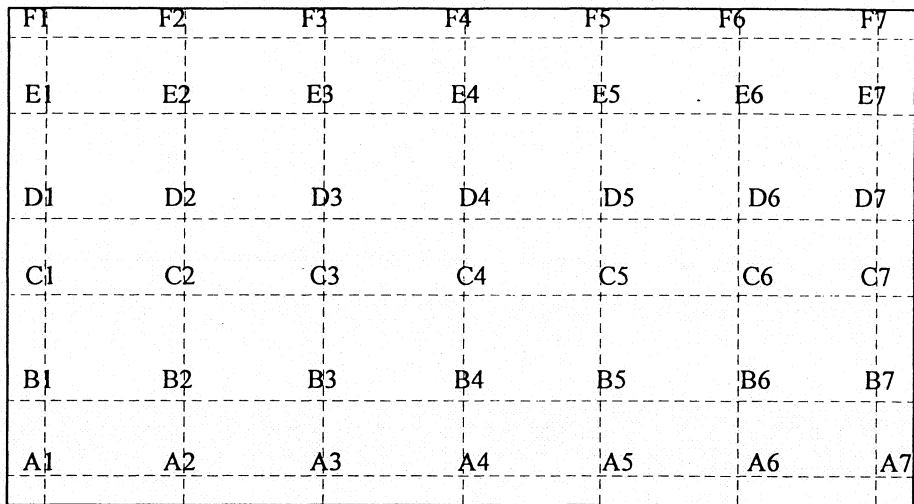


**Figure 3.3 Sensor Locations for the FRP Bridge**

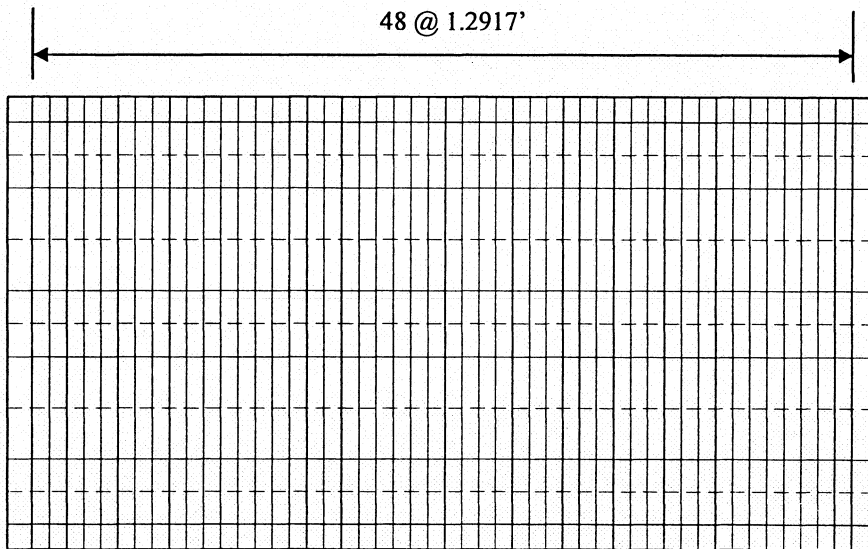
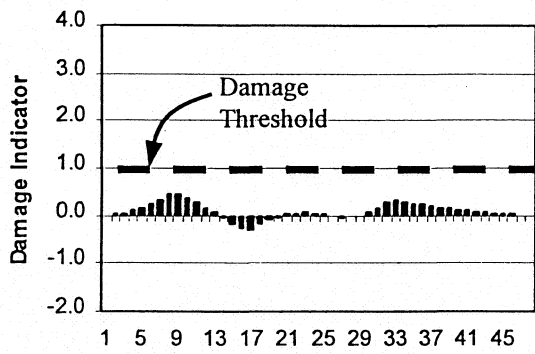
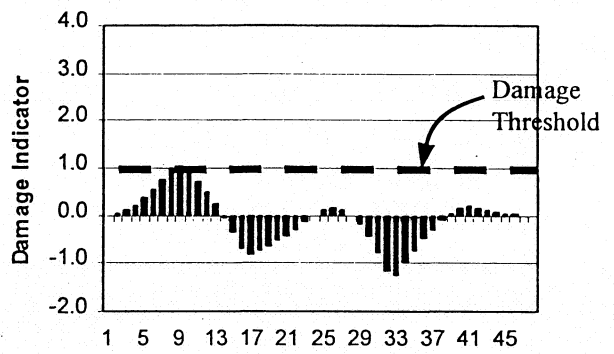


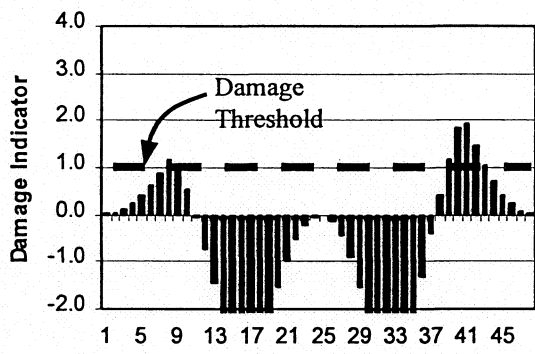
**Figure 3.4 The Damage Detection Model for the FRP Bridge**



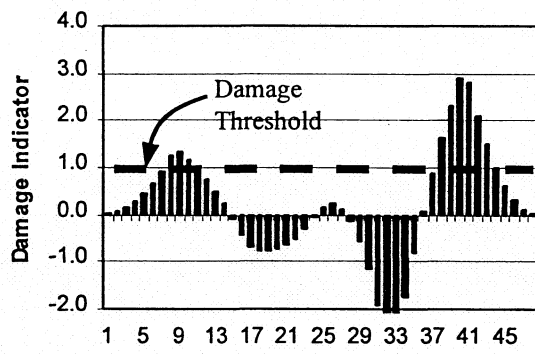
(a)



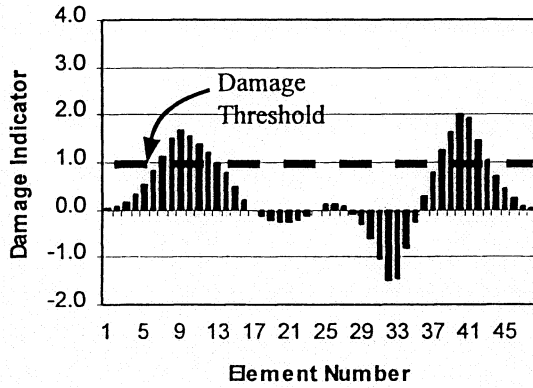
(b)



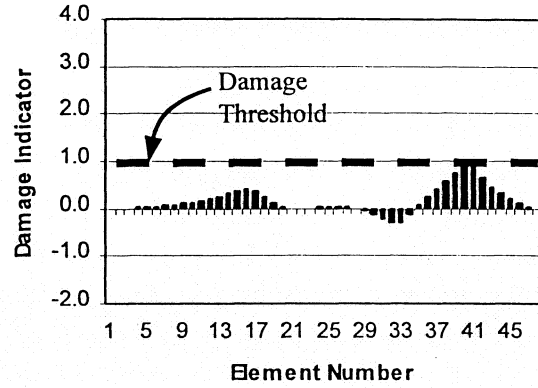
(c)



(d)



(e)



(f)

**Figure 3.5 Damage Localization Results using the First Field Bending Mode and the First Bending Mode of Baseline FRP Model: (a) Result using the Measurement along the Sensors A1 - A7; (b) Result using the Measurement along the Sensors B1 - B7 ; (c) Result using the Measurement along the Sensors C1 — C7; (d) Result using the Measurement along the Sensors D1 — D7; (e) Result using the Measurement along the Sensors E1 - E7; (f) Result using the Measurement along the Sensors F1 — F7**

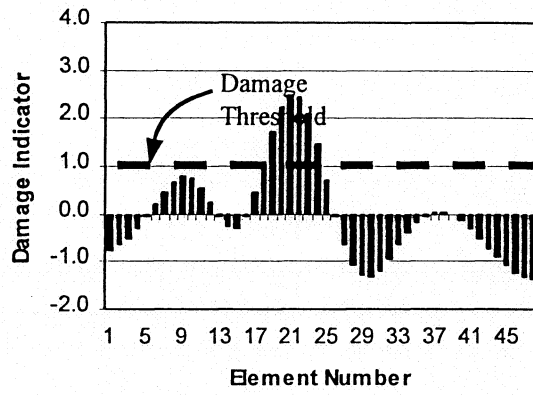
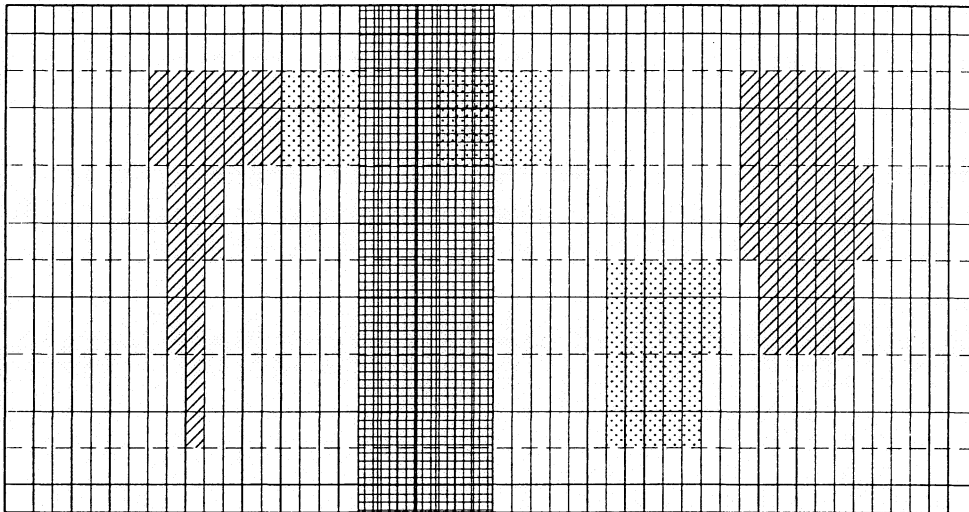


**Figure 3.6 Damage Localization Results using the First Torsional Modes From the Field Data and the Baseline FRP Model**

CL



 Possible Damage Locations Using First Bending

 Possible Damage Locations Using Second Bending

 Possible Damage Locations Using Torsional Mode

**Figure 3.7 Damage Localization Results using the First Bending And Torsional Modes**

#### 4.0 SUMMARY AND CONCLUSIONS

The objective of this report was to describe the system identification and nondestructive damage evaluation of two recently constructed bridges in southern California. The first structure is a conventional two-span monolithic reinforced concrete structure while the second structure, with almost identical superstructure geometry of the first structure, is a composite structure consisting of reinforced concrete, light weight concrete, and various combinations of fabric reinforced plastics. Acceleration-time data for the structures were acquired in the field between 5/3/01 and 5/5/01. Next, modal parameters were extracted from the field data. Finite element models of the structures were then developed to aid in the interpretation of the field data. The field data and the finite element models were combined to produce more detailed finite element models of the structures. Treating the modal parameters of the updated finite element models and the extracted modal parameters from the field tests as the undamaged and the damaged specimens, respectively, a nondestructive damage detection of the as-built structures was performed. A methodology to fine-tune (update) a finite element model of a structure using field frequency data has been demonstrated. Assuming that the mode shapes of the updated structures represent the flawless pristine structures, the numerically generated mode shapes can be used in conjunction with the measured mode shapes to interrogate the newly constructed bridges for possible flaws. This study utilized two measured and numerically generated mode shapes and identified several potential locations of damage in the newly constructed bridges.

## REFERENCES

- [1] ABAQUS (1994). *Version 5.4 User Manual*. Hibbitt, Karlsson & Sorensen, Inc., Providence, Rhode Island.
- [2] Farrar, C., and Jauregui, D., (1996). "Damage Detection Algorithms Applied to Experimental and Numerical Modal Data from the I-40 Bridge." Report No. LA13074-MS, Los Alamos National Laboratory, Los Alamos, New Mexico.
- [3] Gibson, J.D., and Melsa, J.L., (1975). *Introduction to Nonparametric Detection with Applications*, Academic Press, New York, New York.
- [4] Nadler, M., and Smith, E.P., (1993). *Pattern Recognition Engineering*, John Wiley, New York, New York.
- [5] Stubbs, N., and Kim, J.T. (1996), "Damage Localization in Structures without Baseline Modal Parameters," *AIAA J.*, 34(8), 1644-1649.
- [6] Stubbs, N., and Osegueda, R., (1990). "Global Non-Destructive Damage Evaluation in Solids," *Int. J. Analytical and Experimental Modal Analysis*, 5(2), 67-69.
- [7] Stubbs, N., Park, S., Bolton, R.W., Choi, S., and Sikorsky, C. (1999). "Nondestructive Estimate of the Rate of Change of Structural Degradation of the Lavic Road Overcrossing," Final Report #FHWA/CA/ESC/TEES 1-9/99, Caltrans, October.

## APPENDIX I

### SYSTEM IDENTIFICATION USING MODAL SENSITIVITIES AND FREQUENCIES

#### 1.0 The Rationale for the Method

The rationale behind the development of the baseline model can be explained with the aid of Figure 2.1. Suppose a flawed (i.e., damaged) structure [Figure 2.1(a)] is given with field-measured mode shapes  $\Phi_i^*$  and eigenfrequencies  $\omega_i^*$ . Assume that the magnitude of the flaw is small in comparison to a flawless (i.e., baseline) structure. Suppose that an estimate of the flawless structure can be identified, shown in Figure 1.1(b), using only the frequency information from the flawed structure. Then the identified baseline model [Figure 1.1(b)] will have the same eigenfrequencies  $\omega_i^*$  (in the least square sense) of the flawed model [Figure 1.1(a)] but the mode shapes of the two structures will be different in the neighborhood of the flaw. This difference in the mode shapes of the identified baseline structure and the measured mode shapes of the existing structure may then be exploited to localize the flaw.

#### 1.1 The System Identification Methodology

Here, a system identification methodology to identify baseline modal responses of a structure is outlined (Stubbs and Kim 1996). Consider a linear skeletal structure with NE members and N nodes. Suppose  $k_j^*$  is the unknown stiffness of the  $j^{\text{th}}$  member of the structure for which M eigenvalues are known. Also, suppose  $k_j$  is a known stiffness of the  $j^{\text{th}}$  member of a finite element (FE) model for which the corresponding set of M eigenvalues are known. Then, relative to the FE model, the fractional stiffness change of the  $j^{\text{th}}$  member of the structure,  $\alpha_j$ , and the stiffness are related according to the following equation.

$$k_j^* = k_j(1 + \alpha_j) \quad (1)$$

The fractional stiffness change of NE members may be obtained using the following equation (Stubbs and Osegueda 1990):

$$\alpha = F^{-1}Z \quad (2)$$

where  $\alpha$  is a NE x 1 matrix containing the fractional changes in stiffness between the FE model and the structure,  $Z$  is a M x 1 matrix containing the fractional changes in eigenvalues between the two systems, and  $F$  is a M x NE sensitivity matrix relating the fractional changes in stiffness to the fractional changes in eigenvalues.

The M x NE,  $F$  matrix can be determined as follows: first, M eigenvalues are numerically generated from the initial FE model; second, the stiffness of the first member of the FE model is modified by a known amount; third, the corresponding set of M eigenvalues are numerically generated for the modified FE model; fourth, the fractional changes between the M initial eigenvalues and M eigenvalues of the modified structure are computed; fifth, each component of the first column of the  $F$  matrix (i.e., the M x 1,  $F$  matrix) is computed by dividing the fractional changes in each eigenvalue by the magnitude of the modification at member one; and finally, the M x NE,  $F$  matrix is generated by repeating the entire procedures for all NE members.

## 1.2 The System Identification Algorithm

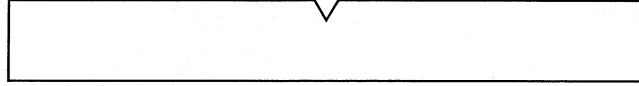
Using the above rational as a basis, the following 6-step algorithm is proposed to identify a given structure:

1. Select a target structure (e.g., a post-damage state of the structure) for which sufficient eigenfrequencies that can be used to identify the baseline structure are available. (Note that the mode shapes of the damaged structure in defining the target structure are ignored.)
2. Select an initial FE model of the structure, utilizing all possible knowledge about the design and construction of the structure.
3. As outlined above, compute the sensitivity matrix of the FE model.
4. As outlined above, compute the fractional changes in eigenvalues between the FEE model and the target structure.

5. Fine-tune the FE model by first solving Equation (2.2) to estimate stiffness changes (i.e., to compute the  $N \times 1$ ,  $\alpha$  matrix) and next solving Equation (2.1) to update the stiffness parameters of the FE model.
6. Repeat steps 1-5 until  $\mathbf{Z} \cong 0$  or  $\alpha \cong 0$  (i.e., as they approach zero) when the parameters of the FE model are identified.

The converged FE model is the baseline model. It has the frequencies of the damaged (i.e., target) structure but none of its members are damaged. Furthermore, the mode shapes of the baseline model differ from those of the damaged structure. Once the baseline model is identified, its modal parameters can be numerically generated [e.g., using commercial software ABAQUS (1994)].

(a) Flawed Structure:  $\Phi_i^*, \omega_i^*$



(b) Estimate of Flawless Structure:  $\Phi_i, \omega_i^*$

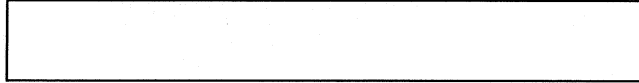


**Figure 2.1 Flawed Structure and Estimate of Flawless Structure**

## APPENDIX II

### THE DAMAGE INDEX METHOD

#### 2.0 Overview

This section summarizes the theory of the damage localization and severity estimation to be used in this project

#### 2.1 General Formulation for Damage Localization

In the field of Nondestructive Damage Detection (NDD) using modal parameters, one of the more difficult problems is that of making a statement regarding the integrity of a relatively small portion of a structure when very few modal parameters are available. In such cases, inverse methods using systems of equations usually result in unsolvable systems with few equations but many unknowns. The discipline of pattern recognition provides a way to deal with such heavily underdetermined systems (Nadler and Smith 1993).

In pattern recognition, physical world data are transduced into the so-called pattern space. Using techniques of dimensionality reduction, the pattern space is reduced to a smaller dimension known as the feature space. Data in the feature space are introduced to a decision algorithm and the elements of the feature space are classified into a finite number of clusters. In the problem at hand, the dynamic response of the structure in the time domain represents the physical world data and the modal parameters represent the pattern space. The feature space is represented by indicators that are a function of measurable pre-damage and post-damage modal parameters. These indicators can be selected in such a manner that they reflect internal structure in the data. The decision algorithm is a means by which the data space is partitioned into  $D_n$  cluster (decision spaces). In this study,  $n=2$  and the decision spaces correspond to the cases: (a) a structure is not damaged at a given location, and (b) a structure is damaged at a given location. For each instance the indicator of damage will fall into one of the two categories.

The damage index method utilizes the change in mode shapes of the pre-damage and post-damage structure to detect and locate damage in a structure (Stubbs et al. 1992). Consider a linear, undamaged, skeletal structure with  $NE$  elements and  $N$  nodes. After

writing the equations of motion for the structure and solving the eigenvalue problem, the  $i^{\text{th}}$  modal stiffness,  $K_i$ , of the arbitrary structure is given by

$$K_i = \Phi_i^T C \Phi_i \quad (2.1)$$

Where  $\Phi_i$  is the  $i^{\text{th}}$  modal vector and  $C$  is the system stiffness matrix. From matrix structural analysis, the contribution of the  $j^{\text{th}}$  member to the  $i^{\text{th}}$  modal stiffness,  $K_{ij}$ , is given by

$$K_{ij} = \Phi_i^T C_j \Phi_i \quad (2.2)$$

where  $C_j$  is the contribution of the  $j^{\text{th}}$  member to the system stiffness matrix. The fraction of modal energy for the  $i^{\text{th}}$  mode that is concentrated in the  $j^{\text{th}}$  member (i.e., the element sensitivity of the  $j^{\text{th}}$  member to the  $i^{\text{th}}$  mode) is given by

$$F_{ij} = K_{ij}/K_i \quad (2.3)$$

Let the corresponding modal parameters in Equations (2.1) to (2.3) associated with a subsequently damaged structure be characterized by asterisks. Then for the damaged structure,

$$F_{ij}^* = K_{ij}^*/K_i^* \quad (2.4)$$

where  $K_{ij}^*$  and  $K_i^*$  are given by, respectively

$$K_{ij}^* = \Phi_i^{*T} C_j^* \Phi_i^* \quad (2.5)$$

and

$$K_i^* = \Phi_i^{*T} C^* \Phi_i^* \quad (2.6)$$

Again, from matrix structural analysis, the contribution of the  $j^{\text{th}}$  member to the stiffness matrices  $C_j$  and  $C_j^*$  in Equations (2.2) and (2.5) may be written as follows:

$$C_j = k_j C_{j0} \quad (2.7)$$

and

$$C_j^* = k_j^* C_{j0} \quad (2.8)$$

where the scalars  $k_j$  and  $k_j^*$ , respectively, are parameters representing the material stiffness properties of the undamaged and damaged  $j^{\text{th}}$  member of the structure, and the matrix  $C_{j0}$  involves only geometric quantities (and possibly terms containing Poisson's ratio). The quantities  $F_{ij}$  and  $F_{ij}^*$  are related by the equation:

$$F_{ij}^* = F_{ij} + dF_{ij} \quad (2.9)$$

where  $dF_{ij}$  is related to the change in the fraction of modal energy of the  $j^{\text{th}}$  member in the  $i^{\text{th}}$  mode. The quantity  $dF_{ij}$  can be obtained from the expression:

$$dF_{ij} = \frac{K_{ij}}{K_i} \left[ \frac{dK_{ij}}{K_{ij}} - \frac{dK_i}{K_i} \right] \quad (2.10)$$

Assuming that the structure is damaged at a single location  $j$  and the resulting change in  $F_{ij}$  is only a function of  $k_j$ , a first order approximation of  $dK_{ij}$  can be obtained from the expression:

$$dK_{ij} \cong \frac{\partial K_{ij}}{\partial k_j} dk_j + \frac{\partial K_{ij}}{\partial u_{ij}} \frac{\partial u_{ij}}{\partial k_j} dk_j \quad (2.11)$$

where

$$u_{ij} = \Phi_i^T C_{j0} \Phi_i \quad (2.12)$$

Using Equations (2.2) and (2.7), it can be shown that

$$\frac{\partial K_{ij}}{\partial k_j} = u_{ij} \quad (2.13)$$

and

$$\frac{\partial K_{ij}}{\partial u_{ij}} = k_j \quad (2.14)$$

Next, introducing the modal force vector associated with the  $j^{\text{th}}$  member and the  $i^{\text{th}}$  mode,  $A_{ij}$ , given by

$$A_{ij} = C_j \Phi_i \quad (2.15)$$

It can be shown that by using Equations (2.7), (2.13), and (2.15),

$$u_{ij} = \frac{1}{k_j^2} A_{ij}^T C_{jo}^{-1} A_{ij} \quad (2.16)$$

Therefore, if it is assumed that the modal force  $A_{ij}$  remains constant while  $k_j$  changes (note that the assumption is true in the case of a statically determinant system), then

$$\frac{\partial u_{ij}}{\partial k_j} = -\frac{2u_{ij}}{k_j} \quad (2.17)$$

Since it has been assumed that the structure is damaged in only one location, it follows readily that  $dK_{ij} = dK_i$ . Also, since  $K_i \gg K_{ij}$ , from Equation (2.10)

$$dF_{ij} \cong \frac{dK_{ij}}{K_i} = -\frac{u_{ij}}{K_i} = -\frac{u_{ij}}{K_i} dk_j = -F_{ij} \alpha_j \quad (2.18)$$

where  $\alpha_j = dk_j/k_j$ , the fractional change in the stiffness of Element  $j$ . Substituting the result of Equation (2.18) into Equation (2.9), and substituting for  $F_{ij}^*$  using Equations ( ) to ( ), it can be shown that

$$\frac{k_j^*}{K_i^*} = k_j \frac{u_{ij}}{K_i} (1 - \alpha_j) \quad (2.19)$$

Substituting for  $\alpha_j = (k_j^* - k_j)k_j$  in Equation (2.19), and rearranging, one obtains:

$$\frac{k_j}{k_j^*} = \left( \frac{u_{ij}^*}{K_i^*} + \frac{u_{ij}}{K_i} \right) / 2 \frac{u_{ij}}{K_i} \quad (2.20)$$

Setting  $f_{ij}^* = u_{ij}^*/K_i^*$  and  $f_{ij} = u_{ij}/K_i$ , Equation (2.20) reduces to

$$DI_{ij} = \frac{k_j}{k_j^*} = \frac{f_{ij}^* / f_{ij} + 1}{2} \quad (2.21)$$

where  $DI_{ij}$  is the indicator of damage in the  $j^{\text{th}}$  member using the  $i^{\text{th}}$  mode. If  $DI_{ij} > 1$ , damage may exist. From Equation (2.21), the fundamental indicator of damage is the quotient  $f_{ij}^*/f_{ij}$ . Note that the one in the numerator is, essentially, a shifting factor while the two in the denominator is a scaling factor. Equation (2.21) becomes singular when  $f_{ij} \rightarrow 0$ : a condition which will occur when, simultaneously, the element size approaches zero and the element is located at a node of a mode. Here the division-by-zero difficulty can be overcome by simply shifting the axis of reference for the sensitivities. For example, if the origin is shifted from  $f_{ij} = 0$  to  $f_{ij} = -1$ , then

$$f_{ij}' \rightarrow 1 + f_{ij} \quad (2.22)$$

and

$$f_{ij}^{*'} \rightarrow 1 + f_{ij}^* \quad (2.23)$$

So the new indicator function,  $DI_{ij}$ , which will also form the basis of feature space (in the pattern recognition sense), becomes

$$DI_{ij} = \frac{f_{ij}^* + 1}{f_{ij} + 1} \approx \left[ \frac{\Phi_i^{*T} C_{j_0} \Phi_i^* + \Phi_i^{*T} C \Phi_i^*}{\Phi_i^T C_{j_0} \Phi_i + \Phi_i^T C \Phi_i} \right] \frac{\Phi_i^T C \Phi_i}{\Phi_i^{*T} C \Phi_i^*} \quad (2.24)$$

There are two important characteristics of the indicator  $DI_{ij}$  given by Equation (2.24): first, the expression attempts to express the changes in stiffness at a specific location in terms of measurable pre-damage and post-damage mode shapes ( $\Phi_I$  and  $\Phi_I^*$ ); and second, the term  $C_{j_0}$  on the right hand side of Equation (2.24) can be determined from a knowledge of the geometry of the structure. Thus for each damage location  $j$ , there are as many  $DI_{ij}$ 's available as there are mode shapes. As noted above, in the context of pattern recognition, the latter values of  $DI_{ij}$  define the feature space. The following expression will be the convenient form of damage index  $DI_j$  for a single location if several modes (NM) are used

$$DI_j = \frac{k_j}{k_j^*} = \frac{\sum_{i=1}^{NM} (\Phi_i^{*T} C_{j_0} \Phi_i^* + \Phi_i^{*T} C \Phi_i^*) \Phi_i^T C \Phi_i}{\sum_{i=1}^{NM} (\Phi_i^T C_{j_0} \Phi_i + \Phi_i^T C \Phi_i) \Phi_i^{*T} C \Phi_i^*} \quad (2.25)$$

The final step in damage localization is classification. Classification analysis addresses itself to the problem of assigning an object to one of a number of possible groups on the basis of observations made on the objects. In this study, the objects are the members of the structure. There are two groups: undamaged elements and damaged elements. Finally, the observations made on the objects are the  $DI_j$ 's. Many techniques are available to accomplish the end. Examples of these methods include classification on the basis of: (1) Bayes' rule (from which the well known Linear Discriminant Analysis and Quadratic Discriminant Analysis are derived), (2) nearest distance, and (3) hypothesis testing (Gibson and Melsa 1975). Currently, the authors have utilized primarily techniques from hypothesis testing. The criteria for damage localization is established based on statistical reasoning. The values,  $DI_1, DI_2, DI_3, \dots, DI_{NE}$  for each element, are considered as realization of a random variable. The standardized damage indicator is given by:

$$z_j = \frac{DI_j - \mu_{DI}}{\sigma_{DI}} \quad (2.26)$$

where  $\mu_{DI}$  and  $\sigma_{DI}$  represent mean and standard deviation of the damage index,  $DI_j$ , respectively. Let  $H_0$  be the hypothesis that structure is not damaged at member  $j$ , and let  $H_1$  be the hypothesis that structure is damaged at member  $j$ . The following decision rules may be used to assign damage to member  $j$ : (1) choose  $H_1$  if  $z_j \geq 2$  and (2) choose  $H_0$  if  $z_j < 2$ .

#### 4.2 Damage Severity Estimation

Note that in Equation (2.25) the indicator of damage is the ratio of the undamaged stiffness to the damaged stiffness. Such a number exists for each potentially damaged member. For example, in the case of a truss there is a  $DI_j$  associated with every member  $j$ . Here the damage is expressed as the fractional change in stiffness of an element:

$$\alpha_j = \frac{k_j^* - k_j}{k_j} = \frac{1}{DI_j} - 1 \quad (2.27)$$

Thus if there is no damage,  $\alpha_j = 0$ ; if there is damage,  $\alpha_j < 0$ . Note that if  $\alpha_j = -1$ , all stiffness capacity is completely lost.

#### 4.3 Damage Index for Deck Elements

The damage detection model used in this program utilizes the Euler-Bernouli Beam Model. For an arbitrary 1-D beam with  $n_e$  elements, a damage localization indicator for each potential damage location  $j$  and mode as follows (Stubbs and Kim 1996):

$$\beta_{ji} = \frac{k_j}{k_j^*} = \frac{\left( \int_j [\phi_i^{**}(x)]^2 dx + \int_0^L [\phi_i^{**}(x)]^2 dx \right) \int_0^L [\phi_i^n(x)]^2 dx}{\left( \int_j [\phi_i^n(x)]^2 dx + \int_0^L [\phi_i^n(x)]^2 dx \right) \int_0^L [\phi_i^{**}(x)]^2 dx} = \frac{NUM_{ji}}{DEN_{ji}} \quad (2.28)$$

in which  $\phi_i(x)$  and  $\phi_i^*(x)$  are the pre- and post-damage  $i^{\text{th}}$  mode shapes, and  $k_j$  and  $k_j^*$  are the pre- and post-damage bending of the  $j^{\text{th}}$  stiffness.